الجمهورية الجزائرية الديمقراطية الشعبية

People's Democratic Republic of Algeria

وزارة التعليم العالي والبحث العلمي

Ministry of Higher Education and Scientific Research

جامعة زيان عاشور بالجلفة

Ziane Achour University of Djelfa

كلية العلوم و التكنولوجيا

Faculty of Science and Technology

Department: Electrical Engineering

Order N° : 108/ 2022

Defense authorization N° : 122/2022

DOCTORAL THESIS

3rd Cycle Doctoral (D-LMD)

Presented by

Ibrahim RAHMANI

With a view to obtaining the doctoral diploma in 3rd Cycle Doctoral (D-LMD)

Branch: Electronics

Specialty: Signal Image and Systems

Topic

Synthesis of digital filters based on series approximations

Supported, on 11 /02 / 2023, before the jury composed of:

Last and first name	Grade	Institution of affiliation	Designation
Mr Farid MESSELMI	Professeur	University of Djelfa	President
Mr Lahcène MITICHE	Professeur	University of Djelfa	Supervisor
Mrs Amel baha houda ADAMOU- MITICHE	Professeur	University of Djelfa	Co-Supervisor
Mr Mohamed DJENDI	Professeur	University of Blida	Examiner
Mr Abdelhamid DAAMOUCHE	Professeur	University of Boumerdès	Examiner
Mr Zaki SARI	Professeur	University of Tlemcen	Invited

Djelfa University, FST - 2022

الجمهورية الجزائرية الديمقراطية الشعبية
République Algérienne Démocratique et Populaire
وزارة التعليم العالي والبحث العلمي
Ministère de l'Enseignement Supérieur et de la Recherche Scientifique

جامعة زيان عاشور بالجلفة
Université Ziane Achour de Djelfa

كلية العلوم والتكنولوجيا
Faculté des Sciences et de la Technologie

Département : Génie Electrique

N° d'Ordre : 108/ 2022

Autorisation de Soutenance N° 122/2022

THESE DE DOCTORAT

Doctorat 3ème Cycle (D-LMD)

Présentée par

Ibrahim RAHMANI

En vue de l'obtention du diplôme de Docteur en 3ème Cycle D-LMD

Filière : Electronique

Spécialité : Signal Image et Systèmes

Thème

Synthèse de filtres numérique basée sur les approximations successifs

Soutenue publiquement, le 11 /02 /2023, devant le jury composé de :

Nom et Prénom	Grade	Etablissement de rattachement	Désignation
Mr Farid MESSELMI	Professeur	Université de Djelfa	Président
Mr Lahcène MITICHE	Professeur	Université de Djelfa	Directeur de thèse
Mrs Amel baha houda ADAMOU- MITICHE	Professeur	Université de Djelfa	Co Directeur de thèse
Mr Mohamed DJENDI	Professeur	Université de Blida	Examinateur
Mr Abdelhamid DAAMOUCHE	Professeur	Université de Boumerdès	Examinateur
Mr Zaki SARI	Professeur	Université de Tlemcen	Invité

Université de Djelfa, FST, 2022

Table of Contents

List of Figures

List of Tables

Lists of Acronyms and Symbols

Acronyms

DSP: Digital Signal Processing

IIR: Infinite Impulse Response.

FIR: Finite Impulse Response.

VDFs: Variable Digital Filters.

VLPFs: Variable Low-Pass Filters.

VBPFs: Variable Band-Pass Filters.

VBSFs: Variable Band-Stop Filters.

VHPFs: Variable high-pass Filters.

DTMF: Digital Tone Multiple Frequency

DFG: Data Flow Graph

MAC: Multiplication Accumulation Cycle

MIPS: Million Instruction Per Second

M-D: Multi-Dimensional

ANFs: Adaptive Notch Filters.

LP-LP: Low-Pass-Low-Pass.

LP-HP: Low-Pass-High-Pass.

LP-BP: Low-Pass-Band-Pass.

LP-BS: Low-Pass-Band-Stop.

FPGA: Field-Programmable Gate Array

PE: Peak Error

Symbols

p_i the pole
z_i the zeros
f_c cut-off frequency
f_0 center frequency
δ_1 passband ripple
δ_2 attenuation
B bandwidth
F_e sampling frequency
P_{calcul} power
T_e period frequency
$a_m(\eta)$ the filter coefficients
$b_k(\eta)$ the filter coefficients
ψ_1 variable parameter
ω_0 notch frequency
$E[y^2(n)]$ mean square output
$\boldsymbol{K}$ controllability Gramian
$\boldsymbol{W}$ observability Gramian
$\hat{\xi}_i$ lattice coefficient
$\boldsymbol{\Theta}$ diagonal matrix
K_{ii}diagonal element

$\otimes$ Kronecker product

Abstract

Variable digital filters are widely used in several signal-processing applications because of their capability of self-tuning frequency characteristics, such as the cutoff frequency and the bandwidth. This thesis proposes new state-space formulations of IIR Variable Digital Filters (VDFs) based on frequency transformations. In the first part, we presented a brief overview of digital filters, then a general overview of the recent development in variable digital filters, focusing on the problems of design and realization and application to adaptive filtering. Then, we proceed into the theory of frequency transformation from the viewpoint of the internal properties of filters. In the second part, VDFs were created using a state-space model based on a frequency transformation, which requires the inverse matrix and the square root, leading to high computational costs. Then a new algorithm was implemented to generate the same VDFs absent the complex calculations that utilized negative binomial and Taylor series approximations in a simple state-space formulation. This algorithm provides high-accuracy approximations of the inverse matrix and square root compared to other algorithms that have been developed. Finally, a comparison study is presented between current works and the suggested technique with the help of illustrations from the literature. Thus, the proposed VDFs have high tuning accuracy with respect to finite wordlength effects.

Keywords: Variable Digital Filters, Frequency transformation, State-space representation, Negative binomial series approximation, Taylor series approximation, Finite wordlength effects.

Résumé :

Les filtres numériques variables sont largement utilisés dans plusieurs applications de traitement de signaux en raison de leur capacité à régler eux-mêmes les caractéristiques de fréquence, telles que la fréquence de coupure et la bande passante. Cette thèse propose de nouvelles formulations d'espace d'état de filtres numériques variables RII (FNV) basées sur des transformations fréquentielles. Dans la première partie, nous avons présenté un bref aperçu des filtres numériques, puis un aperçu général de l'évolution récente des filtres numériques variables, en mettant l'accent sur les problèmes de conception et de réalisation et d'application au filtrage adaptatif. Ensuite, nous passons à la théorie de la transformation de fréquence du point de vue des propriétés internes des filtres. Dans la deuxième partie, les FNV ont été créés à l'aide d'un modèle d'espace d'état basé sur une transformation en fréquence, qui nécessite la matrice inverse et la racine carrée, ce qui entraîne des coûts de calcul élevés. Ensuite, un nouvel algorithme a été mis en œuvre pour générer les mêmes FNV en l'absence des calculs complexes qui utilisaient des approximations binomiales négatives et des séries de Taylor dans une formulation simple d'espace d'état. Cet algorithme fournit des approximations de haute précision de la matrice inverse et de la racine carrée par rapport à d'autres algorithmes qui ont été développés. Enfin, une étude comparative est présentée entre les travaux actuels et la technique suggérée à l'aide d'illustrations de la littérature. Ainsi, les FNV proposés ont une grande précision d'accord en ce qui concerne les effets de longueur de mot finie.

Mots clés : Filtres numériques variables, Transformations fréquentielles, Représentation de l'espace d'état, Approximation de séries binomiales négatives, Approximation en série de Taylor, effets de longueur de mot finie.

ملخص:

تُستخدم المرشحات الرقمية المتغيرة على نطاق واسع في العديد من تطبيقات معالجة الإشارات بسبب قدرتها على ضبط خصائص التردد الذاتي، مثل تردد القطع وعرض النطاق الترددي. تقترح هذه الأطروحة صيغ جديدة لفضاء الحالة للمرشحات الرقمية المتغيرة بناءً على تحولات التردد. في الجزء الأول، قدمنا لمحة عامة موجزة عن المرشحات الرقمية، ثم لمحة عامة عن التطور الأخير في المرشحات الرقمية المتغيرة، مع التركيز على مشاكل التصميم والإدراك والتطبيق على الترشيح التكيفي. ثم ننتقل إلى نظرية تحويل التردد من وجهة نظر الخصائص الداخلية للمرشحات. في الجزء الثاني، تم إنشاء مرشحات رقمية متغيرة باستخدام نموذج فضاء الحالة على أساس تحويل التردد، والذي يتطلب المصفوفة العكسية والجذر التربيعي، مما يؤدي إلى ارتفاع التكاليف الحسابية. ثم تم تنفيذ خوارزمية جديدة لتوليد نفس المرشح الرقمي المتغير في غياب الحسابات المعقدة التي استخدمت التقريب ثنائي الحدود السالب وسلسلة تايلور في صياغة بسيطة لفضاء الحالة. توفر هذه الخوارزمية تقريبات عالية الدقة للمصفوفة العكسية والجذر التربيعي مقارنة بالخوارزميات الأخرى التي تم تطويرها. أخيرًا، يتم تقديم دراسة مقارنة بين الأعمال الحالية والتقنية المقترحة بمساعدة الرسوم التوضيحية من الأدبيات. وبالتالي، فإن المرشحات الرقمية المتغيرة المقترحة لها دقة ضبط عالية فيما يتعلق بتأثيرات طول الكلمة المحدودة.

الكلمات المفتاحية:

المرشحات الرقمية المتغيرة, تحويل التردد, تمثيل فضاء الحالة, تقريب سلسلة ثنائية الحد السلبية, تقريب سلسلة تايلور, تاثير طول الكلمة المحدودة.

Dedication

To my mother and my father…

To my brothers and my sisters…

To all members of my family…

To you especially: Abderrazek & Youcef & Aya…

To all my friends…

To all teachers who have contributed to my education since I was 4 years old until today...

And for all persons who contribute to this work.

ACKNOWLEDGEMEN

First and foremost, I would like to thank Allah Almighty who gave us the strength, courage and patience to carry out this thesis work.

I would like to sincerely thank my supervisor, ***Pr. Lahcène MITICHE****, for doing everything from the inception of the project idea to the last step in it, which enabled me to improve and get an understanding on the subject. Without his invaluable advices, this work would not have been possible.*

Also, I am heartily thankful to ***Pr. Amel Baha Houda ADAMOU-MITICHE,*** *for his encouragement, supervision and support.*

I would like to thank the members of the jury who do me the honor of participating in the defense:

– Pr. Farid MESSELMI

– Pr. Mohamed DJENDI

– Pr. Abdelhamid DAAMOUCHE

– Pr. Zaki SARI

Finally, thanks to all those who contributed, from near or far, to the realization of this work.

Publications

Portions of the work described in this thesis have also appeared in:

Journal

- Rahmani, I., Mitiche, L., & Adamou-Mitiche, A. B. H. (2022). **Improved state-space all-digital filters via series approximations**. Journal of Circuits, Systems and Computers,vol31,N13.

General introduction

Digital Signal Processing (DSP) is interested in representing signals in digital form, processing these signals and the information they carry. Since the early 1970s, when the first DSP chips were introduced, the digital signal processing field has evolved considerably. Digital signal processing has become an integral part of many commercial products and applications and has become a popular term. DSP is useful in almost any application that requires high-speed processing of a large amount of numerical data. Data can be anything from location and speed information for the closed-loop control system to 2D video images to digital sound and vibration signals [1].

In signal processing, signals with unwanted information, such as random noise or interference, are often encountered, or there is a need to selectively extract an interesting signal integrated with many other signals. Filters, in these cases, are used to separate attention signals from others. Filters can be analog or digital. Analog filters use electronic circuits to produce the desired filtration effect, while digital filter uses a digital processor to make digital calculations on signal sample values. The processor may be a general-purpose computing machine, such as a PIC microcontroller or specialized DSP chip. There are two basic types of digital filters: Infinite Impulse Response Filter (IIR) and Finite Impulse Response Filter (FIR).

Variable Digital Filters (VDFs) are frequency selective digital filters capable of real-time tuning of frequency characteristics, such as low-pass filters with tunable cutoff frequency and band-pass filters with tunable center frequency and/or tunable bandwidth. VDFs are widely used in a number of practical applications such as audio processing, telecommunications, and biomedical signal processing systems. Up to the present, a number of research results on VDFs have been proposed, ranging from theoretical framework for design/synthesis to hardware implementation and practical applications [2]. Historically, two approaches are well-known for the design of VDFs. One is the transformation-based technique [3–5], and the other is the spectral parameter approximation-based technique [6–10]. Both techniques have advantages and

disadvantages in practical use. In recent years, these two techniques have been further extended, and new VDFs with low implementation complexity have been proposed [11,12]with applications to reconfigurable filter bank [13,14]and dynamic spectrum learning and access-based cognitive radio networks [15]. Also, in [16–18] another promising technique has been developed for designing VDFs using a fast filter bank approach.

This thesis focuses on the transformation-based technique among the abovementioned techniques. Specifically, we consider VDFs with Infinite Impulse Response (IIR) transfer functions given by the frequency transformation [3]. An advantage of the frequency transformation-based VDFs is the simple mechanism for tuning frequency characteristics, leading to the development of adaptive notch filters [19,20] and adaptive band-pass/band-stop filters [21]. In addition, the frequency transformation-based VDFs have another powerful advantage: high-accuracy filter structures can be used to realize the transfer functions of VDFs. Up to the present, many VDFs with high-accuracy structures have been proposed [22], enabling us to realize VDFs that reduce the performance degradations caused by the finite wordlength effects such as the coefficient quantization error and the round-off noise. These advantages make the frequency transformation-based VDFs attractive in designing, realizing, and implementing many signal processing applications.

In [23], Variable Low-Pass Filters (VLPFs) based on the state-space approach were presented. This method applies to limited transfer functions with distinct complex conjugate poles. Also, the state-space representation presented by this method is limited to particular realization's: the minimum round-off noise realization and the balanced realization. In [24], Variable Band-Pass Filters (VBPFs) and Variable Band-Stop Filters (VBSFs) can only tune the center frequency. However, this method can be applied to any class of transfer function or state-space representation. The state-space VLPFs and VHPFs proposed in [25] can be applied to arbitrary transfer functions and state-space representations. In addition, the VBPFs and VBSFs can tune both the center frequency and the bandwidth by applying two series approximations to reduce the complexity of both the inverse matrix and the square root. However, this proposed series approximation cannot give a high accuracy approximation, motivated by this observation. To this end, this work

proposes frequency transformation-based VDFs, of which structures show high accuracy regarding the finite word length effects. A new, simple algorithm is used for the VDFs. model and implementation in a state-space representation. The inverse matrix and square root are calculated using the negative binomial and Taylor series approximations in the state-space representation to avoid computational complexity. In addition, this approach makes it possible to improve the accuracy in approximating the inverse matrix and square root [26]. Poor approximation accuracy is caused by large values of the approximation parameters, which degrade VDFs performance, as shown in chapter 5. Furthermore, this proposed method allows us to improve the performance of all VDFs (VLPFs, VHPFs, VBPFs, and VBSFs) concerning finite wordlength effects under all tunable frequency characteristics.

The thesis is organized as follows. Start with some reviews of the digital filters basics. Second, an overview of the recent development of variable digital filters. Then, the technique based on frequency transformation is discussed, and then designing the proposed VDFs using the series approximation approach is outlined. Finally, the last chapter offers various examples to show our proposed method's usefulness and efficiency.

Chapter 1

Introduction to digital filters

1.1 Introduction

It is difficult to give a formal definition of the concept of filtering. The electronic engineer often thinks of a modification of the frequency characteristics of a given input signal. From a theoretical point of view, the frequency domain is coupled to the time domain, so filtering also modifies the response in the latter. To a sequence of samples of a discrete time input signal $x(n)$, a digital filter, defined by its impulse response $h(n)$or by its transfer function $H(z)$ in terms of z, responds with a sequence of samples of an output signal $y(n)$ (Figure 1.1).

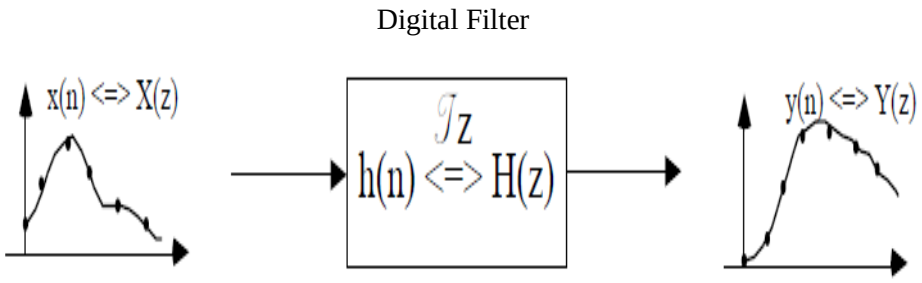

Figure 1.1 Transfer function representation in z.

Examples of filtering are given below.

- Noise reduction for radio signals, sensor images, or audio signals.
- Modification of certain frequency zones in an audio signal or image.
- Limitation to a predefined frequency band.
- Special functions (derivation, integration, Hilbert transform ...).
- In the example of the DTMF (Digital Tone Multiple Frequency) code used in telephony [27], the transmitted signal is the sum of two sinusoids whose frequencies are normalized (see Figure 1.2 left). It results from the choice of the key pressed on

your phone. This principle is often referred to as voice frequencies. At the reception, to recognize the dialed number, a series of filter banks is used (see Figure 1.2 right). A first discrimination of two frequency zones is realized by a high pass filter and a low pass filter. Then, in each zone, a series of band-pass filters followed by a detector allows the presence of a particular frequency to be eliminated.

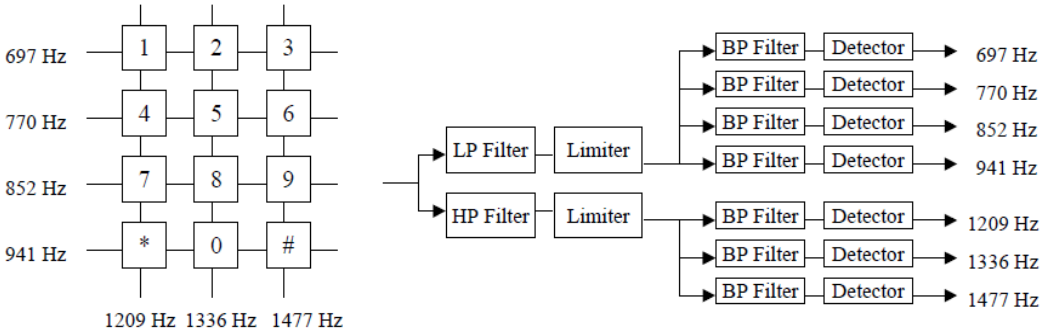

Keypad tone frequencies Tone detection scheme

Figure 1.2 Example of DTMF code in telephony.

1.2 Representation of a digital filter

Digital filtering can be represented using several types of specifications.

1.2.1 Transfer function in z

This representation mode is the most common. It allows to link the input and the output in the plane $\mathcal{Z}$ by $Y(z) = H(z).X(z)$. In the following, we will pose:

$$H(z) = \frac{N(z)}{D(z)} = \frac{\sum_{i=0}^{M} b_i.z^{-i}}{1+\sum_{i=1}^{N} a_i.z^{-i}} \quad (1.1)$$

where $N(z)$ is the polynomial of the numerator of the transfer function, while $D(z)$ is its denominator. N is here the order of the filter. In the case where $H(z)$ has poles, we speak of IIR filters. If $N(z) = 1$ we speak of an all-pole filter. In the case where $D(z) = 1$ the filter has only zeros. This family of filters corresponds to the case of FIR filters. This one has no equivalent in analog filtering, and we will see that its properties make it a very used function in digital signal processing.

Eq.(1.1) can 'also be represented by highlighting the poles and zeros.

$$H(z) = b_0 \frac{\prod_{i=1}^{M=1}(z-z_i)}{\prod_{i=1}^{N=1}(z-p_i)} \tag{1.2}$$

where p_i are the poles and z_i are the zeros of $H(z)$. We recall here that the stability of the filter will be terminated by the poles belonging to the unit circle (i.e. $|p_i| < 1$), and that zeros belonging to the unit circle will characterize a minimum phase filter. Figure 1.3 shows several versions of representations of $H(z)$. The direct form Figure 1.3(a) can be a product or sum of lower order transfer functions, usually of order 2. Eq.(1.3) and Figure 1.3(b) represent the parallel form, while Eq.(1.4) and Figure 1.3(c) represent the cascade form.

$$H(z) = \sum_{i=1}^{M} H_i(z) = \sum_{i=1}^{M} \frac{b_0+b_1z^{-1}+b_2z^{-2}}{1++a_1z^{-1}+a_2z^{-2}} \tag{1.3}$$

$$H(z) = \prod_{i=1}^{M} H_i(z) = \prod_{i=1}^{M} \frac{b_0+b_1z^{-1}+b_2z^{-2}}{1++a_1z^{-1}+a_2z^{-2}} \tag{1.4}$$

1.2.2 Impulse response

The impulse response is the function in z inverse of $H(z)$.

$$H(z) = \sum_{n=0}^{\infty} h(n).z^{-n} \tag{1.5}$$

As in analog filtering, the output of a filter $y(nT)$ is the result of the convolution of the input signal represented in a temporal way $x(nT)$ with the impulse response of the filter $h(nT)$. We have then $y(nT) = x(nT) * h(nT)$ or, if we ignore the sampling period :

$$y(n) = x(n) * h(n) = \sum_{k=0}^{\infty} x(k).h(n-k) = \sum_{k=0}^{\infty} x(n-k).h(k) \tag{1.6}$$

In the case where $x(n)$ is an impulse $\delta(n)$, we find well $y(n) = h(n)$.

According to the cases where $h(n)$. Is infinite or finite support, we will find respectively the two IIR and FIR filter types.

1.2.3 Difference equation

A transformation in z transformation of Eq.(1.1) leads to the following form:

$$y(n) = \sum_{i=0}^{M} b_i . x(n-i) - \sum_{i=0}^{N} a_i . y(n-i) \tag{1.7}$$

We identify here two distinct parts: a part depending on the current value and the previous values of the input $x(n)$and a part depending on the previous values of the output $y(n)$. Depending on whether the ai are non-zero or zero, we will speak of recursive or non-recursive filters.

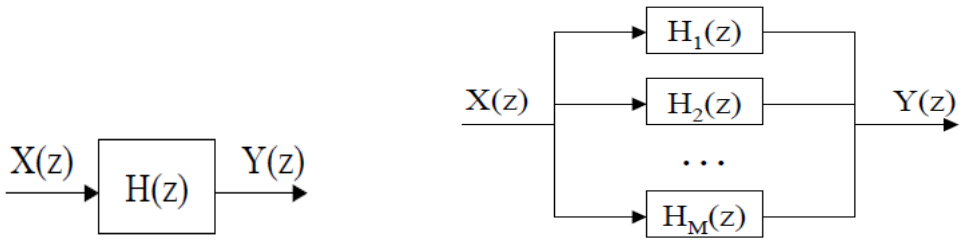

a) Direct form b) Parallel form

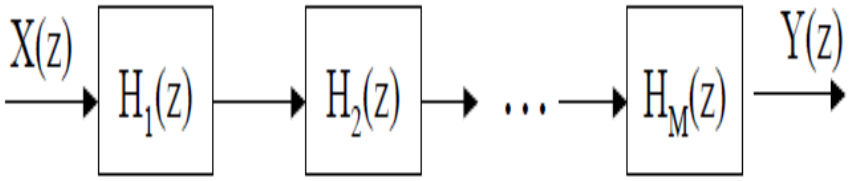

c) Cascade form

Figure 1.3 Transfer function representations in z.

1.3 Specification of a digital filter

Before a digital filter can be designed and implemented, we need to define its specifications. A filter must let certain frequencies pass, while it must attenuate (or even

eliminate) others. We must therefore be able to represent these constraints. There are four basic filters:

- low-pass filters allow frequencies below a cut-off frequency to pass and block those above it Figure 1.4(a). f_c and block those above it Figure 1.4(a),
- high-pass filters block frequencies below a cut-off frequency f_c and let pass those above it Figure 1.4(b),
- band-pass filters allow frequencies around a central frequency f_0 (or between f_1 and f_2) and block the others Figure 1.4(c),
- band-stop filters block frequencies around a center frequency f_0 (or between f_1 and f_2) and let the others pass Figure 1.4(d).

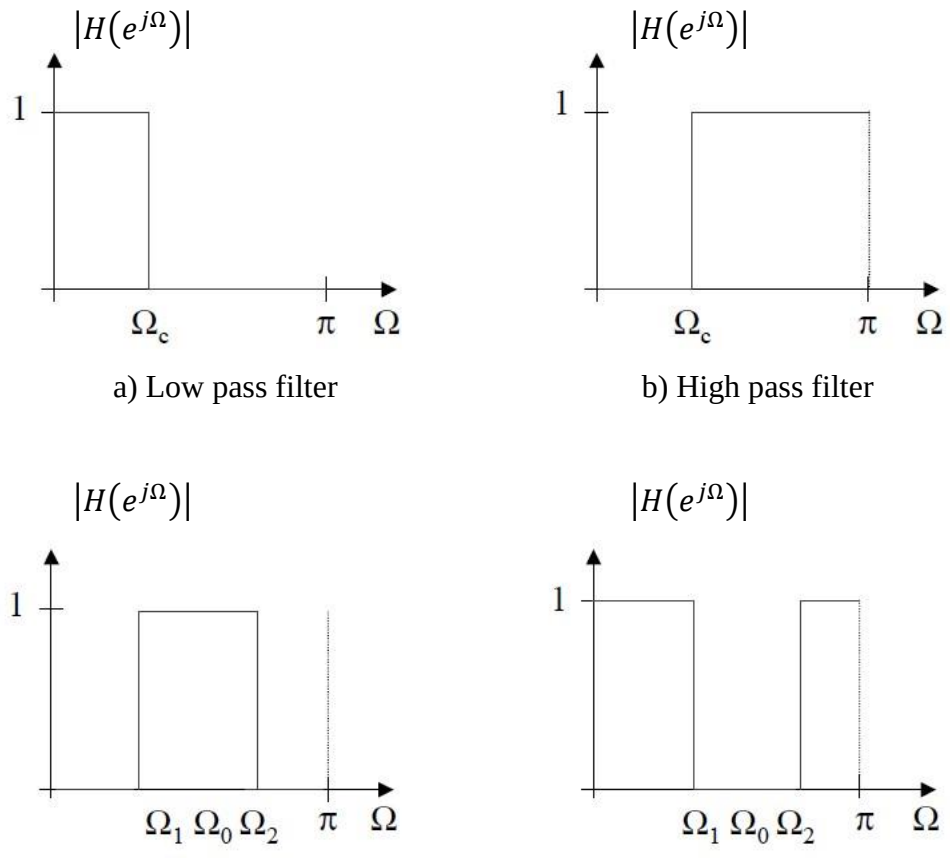

a) Low pass filter b) High pass filter

c) Band-pass filter d) Band-stop filter

Figure 1.4 Ideal frequency responses of the 4 basic filters.

The filters shown in Figure 1.4 are ideal. In a real case there can be no discontinuities. The passage between the passing and attenuated zones is done by the so-called "transition" zones whose width will express the selectivity of the filter. The pass and attenuated bands are also not ideal, they contain ripples whose amplitude is expressed by the parameters of ripple in pass band and attenuation. For all these reasons, the specification of a filter is usually made from a frequency gabarit, defined between 0 and π.

1.3.1 Low-pass and high-pass filter specifications

A low-pass filter has three zones: the pass-band ($0 \leq \Omega \leq \Omega_p$), the transition band ($\Omega_p \leq \Omega \leq \Omega_a$) and the attenuated band ($\Omega_a \leq \Omega \leq \pi$) . Figure 1.5(a) shows a graphical representation of the linear frequency gabarit of a low-pass filter, while Figure 1.5(b) shows a frequency template in dB. A high-pass filter would have its attenuated and pass bands reversed, in this case we would have $\Omega_p > \Omega_a$. δ_1 is the passband ripple, δ_2 is the attenuation.

The selectivity of the filter is defined in table 1.1.

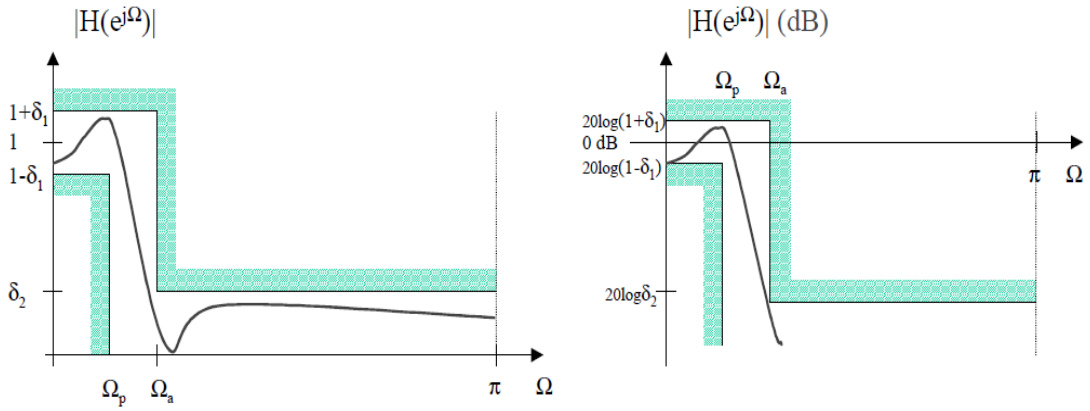

a) Linear frequency gabarit b) Frequency gabarit in dB

Figure 1.5 Frequency gabarit of a low pass filter.

1.3.2 Specifications of band-pass and band-stop filters

A band-pass filter has several zones: the pass-band ($\Omega_{p-} \leq \Omega \leq \Omega_{p+}$), two transition bands and two attenuated bands ($0 \leq \Omega \leq \Omega_{a-}$ and $\Omega_{a+} \leq \Omega \leq \pi$). Figure 1.6 [28] shows a graphical representation of the linear frequency gabarit of a band-pass filter. A band-stop filter would have its attenuated and pass bands reversed.

Table 1.1 summarizes the parameters of the different templates studied [28].

	Low-pass	High-pass	Band-pass	Band-stop
Selectivity s	$\frac{\Omega_p}{\Omega_a}$	$\frac{\Omega_a}{\Omega_p}$	$\frac{\Omega_{p+} - \Omega_{p-}}{\Omega_{a+} - \Omega_{a-}}$	$\frac{\Omega_{a+} - \Omega_{a-}}{\Omega_{p+} - \Omega_{p-}}$
Ripple	δ_1	δ_1	δ_1	δ_1
Attenuation	δ_2	δ_2	δ_2	δ_2
Center frequency Ω_0	—	—	$\sqrt{\Omega_{p+}.\Omega_{p-}}$	$\sqrt{\Omega_{p+}.\Omega_{p-}}$
bandwidth B	—	—	$\frac{\Omega_{p+} - \Omega_{p-}}{\Omega_0}$	$\frac{\Omega_{p+} - \Omega_{p-}}{\Omega_0}$

Table 1.1 Specification parameters of a digital filter.

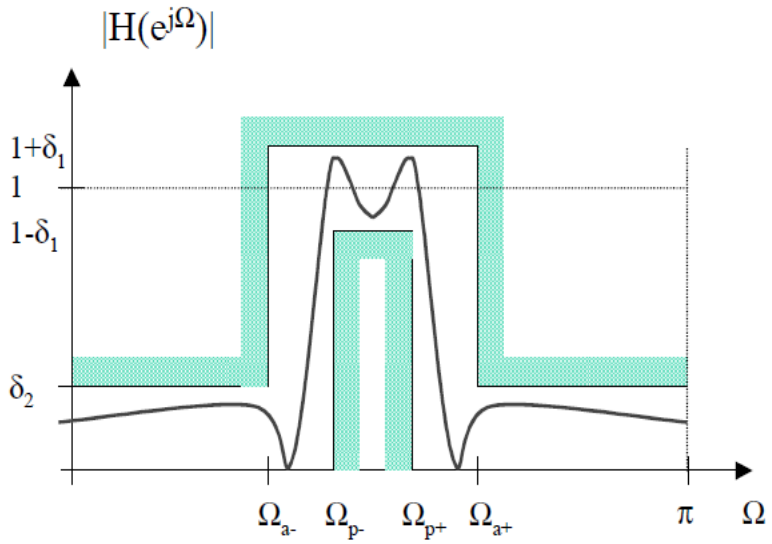

Figure 1.6 Linear frequency gabarit of a band-pass filter.

1.4 Classification of digital filters

Digital filters can be classified according to several criteria:

1- the length of the impulse response involves two types of filters IIR and FIR.
2- the type of representation, or structure, involves two types of recursive filters and non-recursive.

We will see that except for one particular case, recursive and non-recursive filters are respectively equivalent to IIR and FIR filters.

1.4.1 Recursive IIR filters

Analog filters necessarily have an infinite impulse response. Digital IIR filters behave in a similar way, except for the effects due to discretization. This class of filter is also characterized by a transfer function in z containing poles, and a recursive difference equation, i.e. when the output $y(n)$ depends on both the inputs and the previous outputs. Eq.(1.8) and Eq.(1.9) show the transfer function in z and the corresponding difference equation of the general form of an IIR filter. N is called here the order of the filter.

$$H(z) = \frac{N(z)}{D(z)} = \frac{\sum_{i=0}^{M} b_i.z^{-i}}{1+\sum_{i=1}^{N} a_i.z^{-i}} \quad (1.8)$$

$$y(n) = \sum_{i=0}^{M} b_i.x(n-i) - \sum_{i=0}^{N} a_i.y(n-i) \quad (1.9)$$

From Eq.(1.8), two cases arise:

1. if $N(z)$ is not divisible by $D(z)$we have an infinite number of terms in the polynomial division of $N(z)$ by $D(z)$:

$$H(z) = \sum_{n=0}^{N} c_n.z^{-n}$$
$$h(n) = c_n \, for \, n = 0 \ldots \infty$$

$H(z)$ is an IIR filter

2. if $N(z)$ is divisible by $D(z)$then we have a finite number of terms in the polynomial division of $N(z)$ by $D(z)$:

$$H(z) = \sum_{n=0}^{N-1} c_n . z^{-n}$$
$$h(n) = c_n \, for \, n = 0 \ldots N-1$$

$H(z)$ is a FIR filter.

The main features of IIR filters are:

1. a transition band that can be narrow.
2. synthesis methods by transposition of the methods for analog filters.
3. a potential instability due to poles located outside the unit circle (i.e. $|p_i| \geq 1$ regardless of i).
4. A potential numerical instability (i.e. after quantization of the coefficients and the signal) due to the looping.

1.4.2 Non-recursive filters FIR

FIR filters cannot be derived from analog filters. However, they are widely used because they have unique properties (linear phase, stability, flexibility). Eq.(1.10) and Eq.(1.11) show the transfer function in z and the corresponding difference equation of the general form of an IIR filter. N is called here the length of the filter impulse response.

$$H(z) = \sum_{i=0}^{N-1} b_i . z^{-i} \quad (1.10)$$
$$y(n) = \sum_{i=0}^{N-1} b_i . x(n-i) \quad (1.11)$$

We notice by exploiting Eq.(1.11) that the b_i coefficients of the filter are also the values of the impulse response $h(n)$ which is therefore limited in time.

$$H(z) = \sum_{i=0}^{N-1} b_i . z^{-i} \iff h(n) = \sum_{i=0}^{N-1} b_i . \delta(n-i) \quad (1.12)$$
$$h(n) = \begin{cases} b_n & for \; 0 \leq n \leq N-1 \\ 0 & otherwise \end{cases} \quad (1.13)$$

The main characteristics of FIR filters are:

1. A transition band that will always be wider than an IIR filter with the same number of coefficients.
2. synthesis methods allowing to derive any frequency response.
3. inherent stability ($\sum_{n=0}^{N-1}|h(n)| < \infty$).
4. greater numerical stability than IIR.
5. a phase that can be exactly linear, therefore a constant group delay and no harmonic distortion in the signal.
6. Easier implementation in a digital processing system.

1.5 Frequency analysis of digital filters

The frequency analysis is the representation of the transfer function of the filter in the frequency domain, i.e. the Fourier domain. The transfer function is the Fourier transform of the signal $h(n)$.

$$H\left(e^{j\Omega}\right) = \sum_{n=0}^{\infty} h(n).e^{-j\Omega n} = H(z)/z = e^{j\Omega} \qquad (1.14)$$

This function corresponds to a discrete signal, so it is periodic with period 2π. It is for this reason that we usually use the notation $H\left(e^{j\Omega}\right)$ rather than $H(\Omega)$ Figure 1.7 shows an example of a low pass filter. In signal processing, we usually study the modulus and the phase (or argument) of the complex function $H\left(e^{j\Omega}\right)$.

$$H\left(e^{j\Omega}\right) = H_r(e^{j\Omega}) + jH_i\left(e^{j\Omega}\right) = \left|H\left(e^{j\Omega}\right)\right|e^{j\Phi(\Omega)} \qquad (1.15)$$

1.6 IIR and FIR filter structures

1.6.1 FIR filter structure

The structure of a filter is a Data Flow Graph (D.F.G.) in which the nodes are operations (additions are usually represented by circles containing a + and multiplications

by triangles associated with multiplicand coefficients) and the arcs are dependencies, i.e. the data flow from the signal. Some arcs are values

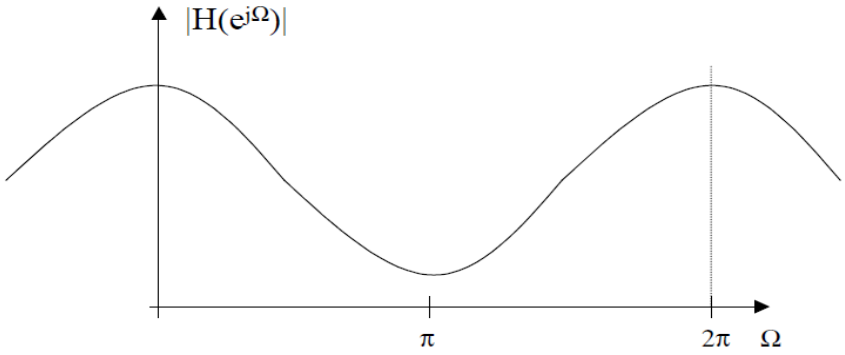

Figure 1.7 Example of a low-pass filter.

A coefficient z^{-1} representing a delay of one sampling period. This coefficient is also represented in the form of a register.

Equation:

$$y(n) = \sum_{i=0}^{N} b_i . x(n-i) = b_0 . x(n) + b_1 . x(n-1) + .. + b_{N-1} . x(n-N+1) + b_N . x(n-N) \quad (1.16)$$

Represents the temporal behavior of an FIR filter. We can immediately deduce the direct structure of an FIR filter which is represented in Figure 1.8(a). The transposed structure of Figure 1.8(b) is obtained after manipulation of this equation.

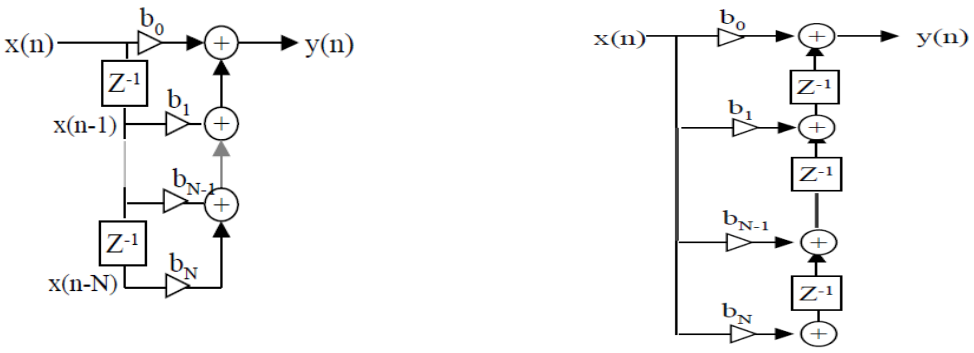

a) Direct structure b) Transposed structure

Figure 1.8 FIR filter structures.

1.6.1.1 Complexity of implementing an FIR filter

A FIR filter does not require $N+1$ multiplication operations, N addition operations for each new sample to be filtered. The complexity can also be expressed in terms of the number of multiplication-accumulation operations (MAC) [28], which, in the case of the FIR filter, is $N+1$. The memory cost of a FIR filter is $2(N+1)(N+1)$ coefficients b_i and $N+1$ memory points for the vector of inputs $x(i)$.

If the sampling frequency of the signal is F_e this means that the calculation of a filter will have to be realized in a time T_{calcul} less than $T_e = \frac{1}{F_e}$.

On a DSP type processor capable of executing a multiplication-accumulation (MAC) at each cycle, of computing power P_{calcul}Calculation expressed in *MIPS* (*Million Instruction Per Second*), the calculation time will be: $T_{calcul} = (N+1).T_{cycle} = (N+1) / P_{calcul}$. Also, the computing power of a DSP for the implementation of a FIR filtering is:

$$P_{calcul}(MIPS) > (N+1).F_e / 10^6 \tag{1.17}$$

1.6.2 IIR filter structure

The following Eq.(1.18) shows that we can represent an IIR $H(z)$ filter as the product of 2 structures, one of which is a FIR $N(z)$filter, and the other one is an *all-pole* IIR filter $1 / D(z)$.

$$H(z) = \frac{N(z)}{D(z)} = [N(z)] \times \left[\frac{1}{D(z)}\right] = \left[\sum_{i=0}^{M} b_i . z^{-i}\right] \times \left[\frac{1}{1+\sum_{i=1}^{N} a_i . z^{-i}}\right] \tag{1.18}$$

The direct structure of an IIR filter is thus obtained by cascading an FIR filter in direct form, and the immediate representation of the all-pole filter $1 / D(z)$. This one is given in Figure 1.9(a). By joining the additions of the center of the Figure, we obtain the classical direct form used in the literature represented in Figure 1.9(b).

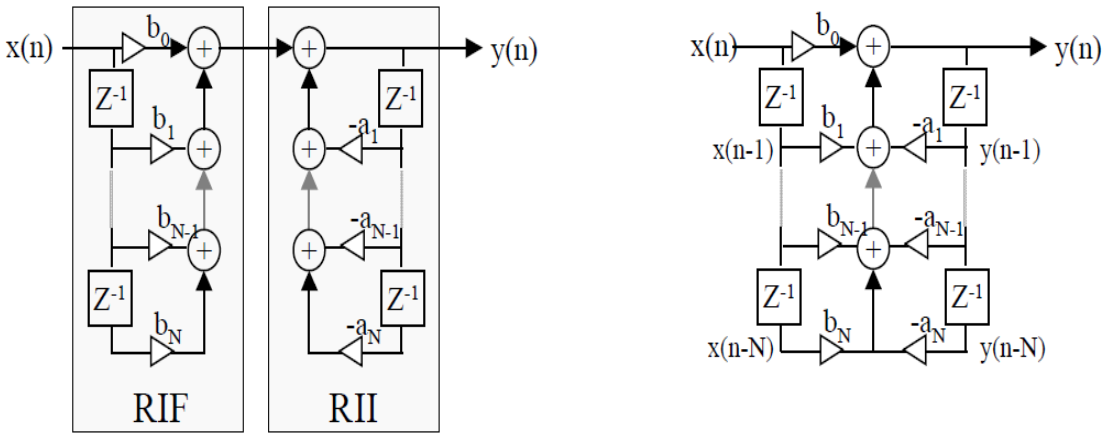

a) Cascade b) Direct structure

Figure 1.9 Direct structures of IIR filters.

It is of course possible to represent an IIR filter differently by using the commutativity property of multiplication. We then have :

$$H(z) = \left[\frac{1}{D(z)}\right] \times [N(z)] = \left[\frac{1}{1+\sum_{i=1}^{N} a_i.z^{-i}}\right] \times \left[\sum_{i=0}^{M} b_i.z^{-i}\right] \qquad (1.19)$$

We can thus exchange on Figure 1.9(a) the 2 blocks FIR and IIR The two delay lines allowing memorizing the signals $x(n)$ being common, it is possible to reunite them by obtaining a unique vector of registers $\omega(n)$ as shown in Figure 1.10(a).

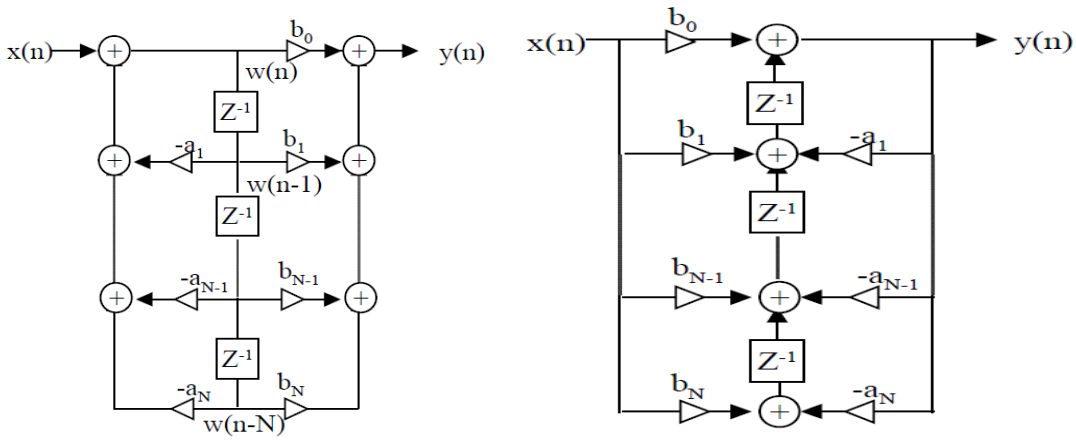

a) Direct canonical structure b) Transposed canonical structure

Figure 1.10 Canonical structures of IIR filters.

The canonical structure can also be represented as a system of Eq.(1.20) showing the signal $\omega(n)$.

$$\begin{cases} W(z) = \frac{1}{D(z)}.X(z) \\ Y(z) = N(z).X(z) \end{cases} \quad \begin{cases} \omega(n) = x(n) - \sum_{i=1}^{N} a_i \omega(n-i) \\ y(n) = \sum_{i=0}^{M} b_i \omega(n-i) \end{cases} \tag{1.20}$$

1.6.2.1 Complexity of implementing an IIR filter

An IIR filter requires $2N + 1$ multiplication operations, $2N$ addition operations for each new sample to be filtered or $2N + 1$ *MAC*. The memory cost of an IIR filter in direct structure is $4N + 3(2N + 1)$ coefficients b_i and $2N + 1$ memory points for the vectors of inputs $x(n)$ and the outputs $y(n)$. The canonical structure allows to decrease the memory cost which only requires $N + 1$ memory points for the vector $\omega(n)$. If the sampling frequency of the signal is F_e this means that the calculation of the filter Must be completed in a time T_{calcul} less than $T_e = \frac{1}{F_e}$.

On a DSP type processor capable of executing a multiplication-accumulation (MAC) at each cycle, of computing power *P* computing expressed in *MIPS (Million Instruction Per Second)*, the computing time will be: $T_{calcul} = (2N + 1).T_{cycle} = (2N + 1) / P_{calcul}$. Also, the computing power of a DSP for the implementation of a FIR filtering is :

$$P_{calcul}(MIPS) > (2N + 1).F_e / 10^6 \tag{1.21}$$

1.7 Conclusion

This chapter covered the definitions, classifications, and specifications of digital filters. Moreover, Finite Impulse Response (FIR) filters and Infinite Impulse Response (IIR) filters were presented and compared, which serves as the foundation for chapter 2, which focuses on recent developments digital filters, design methods, benefits, drawbacks, and types.

Chapter 2

Recent developments in variable digital filters

2.1 Introduction

Digital filter is widely recognized as one of the most basic and necessary components of signal processing systems. In addition, many signal processing applications, such as digital audio equipment and communications systems need the simultaneous implementation of digital filtering and management of filter parameters in real time. Such needs may be satisfied by use of variable digital filters (VDFs). Since the 1970s, several findings have been published about VDFs research. Among these, [2] provides a comprehensive analysis of the outcomes up to the 1990s.

The issues that must be resolved in the creation of VDFs are substantially identical to those that must be resolved in digital filters with set characteristics. Consequently, research concerns on VDFs and fixed characteristic filters are categorized into three groups [26], the approximation problem, the realization problem, and the implementation problem. Additionally, in the realm of VDFs, application-focused outcomes have been actively published. Adaptive notch filters, which have been researched since the 1980s and whose particulars will be discussed in this chapter, are one of the most well-known applications.

In the sequel, initial focus is placed on a summary of VDF foundations. The most recent findings on VDFs are presented and analyzed after that, with the approximation issue, the realization problem, and the applications serving as the primary areas of concentration.

2.2 Fundamentals of VDFs

2.2.1 Definition

VDFs are frequency-selective digital filters (e.g., low-pass filters and band-pass filters) whose frequency properties may be altered in real time through parameter control. Figure 2.1 [25] depicts a common example of such VDFs, the variable low-pass filter (VLPF), whose cutoff frequency may be altered by adjusting the value of a single parameter η , Figure 2.2 [24] also depicts the variable band-pass filter (VBPF), where the bandwidth is constant and the pass-band center frequency may be changed by a single parameter ξ.

It must be noticed that VDFs vary from the "filters with variable (adjustable) coefficients" used in adaptive filtering. Following are the specifics of the differences:

• In the case of general adaptive filtering, an adaptive algorithm modifies all filter coefficients. In contrast, the majority of coefficients in a VDF are either fixed or supplied as functions of just few variable parameters. In the VLPF of Figure 2.1, for instance, only the single parameter is variable, while the remaining coefficients are fixed or supplied as functions of η.

• VDFs vary from standard adaptive filters in terms of the process used to alter frequency characteristics. In VDFs, the characteristics are altered, but the frequency selectivity is maintained, including the low-pass and band-pass shapes. In other words, VDFs regulate the frequency characteristics while preserving the frequency selectivity. In contrast, general adaptive filters do not require this restriction. This indicates that such adaptive filters converge on ideal ones whose properties do not always include frequency selectivity.

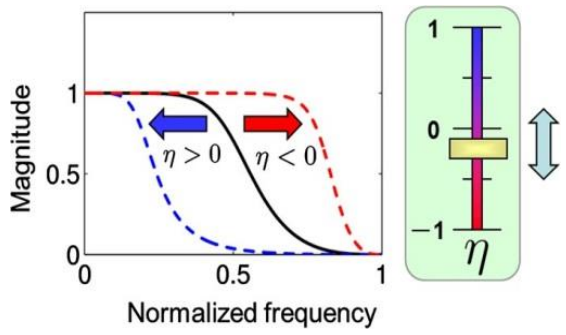

Figure 2.1 Illustration of a VLPF.

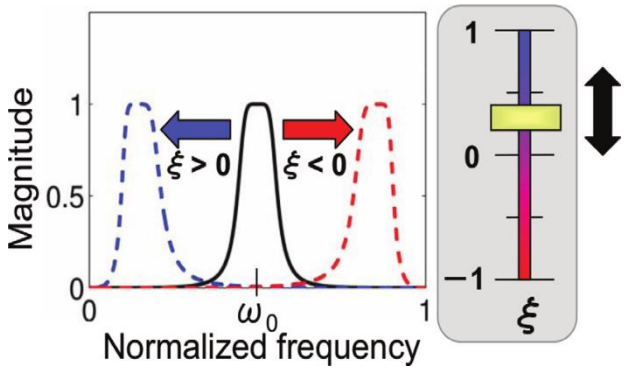

Figure 2.2 Illustration of a VBPF.

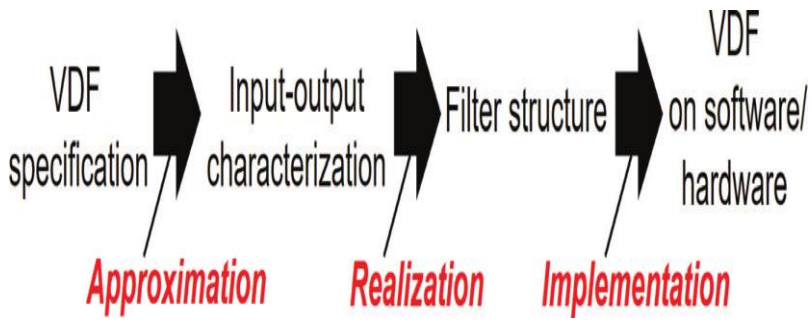

Figure 2.3 Diagram of the steps required to get VDF.

2.2.2 The procedure to obtain VDFs

In this part, we will discuss the process that must be followed to acquire VDFs. The necessary technique is, for the most part, the same as that is needed in the situation of fixed characteristic filters, where it is necessary to take into consideration the three significant challenges depicted in Figure 2.3: approximation, realization, and implementation [49]. In this chapter, we focus a lot of our attention on the issue of

approximation as well as the problem of realization. An input-output characterization, such as a transfer function, must be obtained from a predetermined specification of a VDF in order to solve the approximation issue. The realization issue consists of determining a structure that corresponds to the input-output characterization. This structure may be an adequate collection of adders and multipliers or an appropriate list of basic operations for filtering.

In the VDF approximation problem, it is necessary to incorporate variable parameters in the description of an input-output relationship (e.g., transfer function) of the VDF. Consider, for instance, the approximation issue shown in Figure 2.1 for the VLPF. In order to achieve this VLPF as a FIR filter, one must approximate the transfer function as follows:

$$H(z,\eta) = \sum_{K=0}^{N} h_k(\eta) z^{-k} \tag{2.1}$$

Additionally, each coefficient $h_k(\eta)$ must be described as a function of η. Consequently, the approximation challenge for this VLPF is to identify the set of functions $h_k(\eta)(0 \leq k \leq N)$. similarly, in order to produce IIR-type VLPF, it is essential to characterize the transfer function as:

$$H(z,\eta) = \frac{\sum_{k=0}^{M} b_k(\eta) z^{-k}}{1+\sum_{m=1}^{N} a_m(\eta) z^{-m}} \tag{2.2}$$

and to find the filter coefficients as functions $\{a_m(\eta)\}\,(1 \leq m \leq N) and$ $\{b_k(\eta)\}\,(0 \leq k \leq M)$

2.3 Research topics relating to VDFs

This section presents VDF research problems from the approximation problem and the realization problem perspectives. For the approximation and implementation of VDFs, the variable transformation of transfer functions and the multi-dimensional (M-D) polynomial approximation of filter coefficients have been extensively employed. In the next section, the specifics of these two methodologies are examined, and some recent

findings on them are presented.

2.3.1 VDFs based on variable transfer function transformation

In this procedure, we must first create the transfer function of the "prototype filter," which is often a low-pass filter with preset coefficients (i.e., variable parameters are not included in this transfer function). Next, we apply a variable transformation to this prototype transfer function in order to get the required VDF, where the variable transformation utilizes a function with variable parameters related with the frequency characteristic components to be altered. There are several ways for variable transformations, with the frequency transformation being the most well-known. [3]. All-pass functions are used for the variable transformation in the frequency transformation. Despite the fact that [2] provides a comprehensive overview of the frequency transformation, this chapter will also cover this subject with additional explanations. This is due to the fact that numerous findings using the frequency transformation have been published in recent years.

The analyze the VLPF shown in Figure 2.1 once again. If frequency transformation is employed to generate this VLPF, the transfer function of a prototype low-pass filter must be constructed first. This transfer function is indicated by $H_p(z)$. Then, by performing the following frequency transformation to $H_p(z)$, the necessary VLPF with transfer function $H(z,\eta)$: may be obtained as :

$$H(z,\eta) = H_p(z)\big|_{z^{-1}\leftarrow T(z,\eta)}$$

$$T(z,\eta) = \frac{z^{-1} - \eta}{1 - \eta z^{-1}}. \tag{2.3}$$

Where $T(z,\eta)$ is the all-pass first-order transfer function. By adjusting the value of η in $H(z,\eta)$, the cutoff frequency of the VLPF may be controlled. If $\eta > 0$, the cutoff frequency falls below the frequency of the prototype filter. When $\eta < 0$, the converse holds. If the prototype filter is stable and $|\eta| < 1$ is met, the stability of this VLPF is ensured, also, we note that $\left|T(e^{jw},\eta)\right| = 1$ holds for any η and ω because $T(z,\eta)$ is all-pass.

Next, we will talk about the realization issue for this VLPF. Eq. (2.3) indicates that, from a realization standpoint, a block diagram of this VLPF may be created by substituting each delay element z^{-1} in the prototype filter with the all-pass filter $T(z,\eta)$. In the majority of instances, however, this substitution leads in delay-free loops and a block diagram $H(z,\eta)$ that is not realizable. To understand this issue, consider a second-order IIR prototype filter with the transfer function defined by:

$$H_p(z) = \frac{b_0+b_1z^{-1}+b_2z^{-2}}{1+a_1z^{-1}+a_2z^{-2}} \tag{2.4}$$

Figure 2.4(a), depicts the block diagram derived from the direct form. The VLPF whose block diagram corresponds to Figure 2.4(b) is produced by applying the aforementioned substitution of delay elements with $T(z,\eta)$. It is now evident that Figure 2.4(b) contains delay-free loops; hence, this block design cannot be implemented. It is well know that delay-free loops may be avoided via transfer function or difference equation modifications. However, such manipulations are not effective methods for VDF implementation For example, the transfer function of the second-order VLPF is produced by applying $z^{-1} \leftarrow T(z,\eta)$ to $H_p(z)$ given in Eq. (2.4) and then performing mathematical manipulations [49]:

$$\begin{aligned}
H(z,\eta) &= \frac{b_0'(\eta)+b_1'(\eta)+b_2'(\eta)}{1+a_1'(\eta)+a_2'(\eta)} \\
a_1'(\eta) &= \frac{-2\eta+a_1(1+\eta^2)-2a_2\eta}{1-a_1\eta+a_2\eta^2} \\
a_2'(\eta) &= \frac{\eta^2-a_1\eta+a_2}{1-a_1\eta+a_2\eta^2} \\
b_0'(\eta) &= \frac{b_0-b_1\eta+b_2\eta^2}{1-a_1\eta+a_2\eta^2} \\
b_1'(\eta) &= \frac{-2b_0\eta+b_1(1+\eta^2)-2b_2\eta}{1-a_1\eta+a_2\eta^2} \\
b_2'(\eta) &= \frac{b_0\eta^2-b_1\eta+b_2}{1-a_1\eta+a_2\eta^2}
\end{aligned} \tag{2.5}$$

Using this description to construct the VLPF greatly increases the computational cost, since the filter coefficients $a_1'(\eta), a_2'(\eta), b_0'(\eta), b_1'(\eta), b_2'(\eta)$ must be revised to

account for the change in η. Particularly, the filter coefficients in Eq.(2.5) are rational polynomials that need divisions in order to recalculate filter coefficients, resulting in very expensive implementation.

The Taylor approximation-based description [30] is a prominent way for overcoming this challenge. This approach applies the first-order Taylor series approximation to all rational polynomials of filter coefficients in VDFs, based on the premise that the Taylor series is continuous:

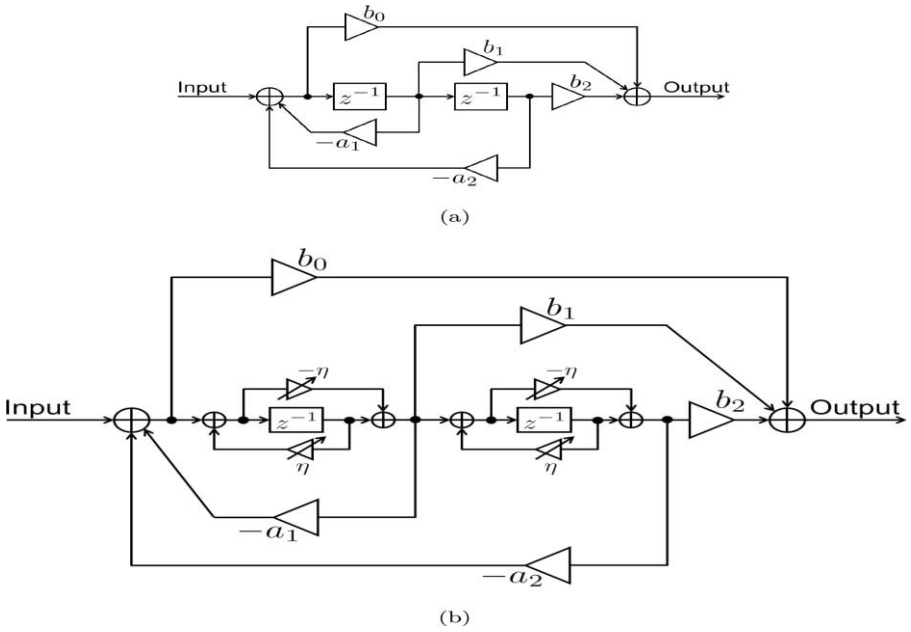

Figure 2.4 Problem in realization of VLPF based on frequency transformation: (a) second-order model filter, and (b) VLPF generated by applying $z^{-1} \leftarrow T(z, \eta)$ to the prototype filter.

Ensure all variable parameters have tiny absolute values. In the case of Eq. (2.5), for instance, it is assumed that $|\eta| \ll 1$ and the filter coefficients are approximated to [30]:

$$\begin{aligned} a_1'(\eta) &\approx a_1 + (a_1^2 - 2 - 2a_2)\eta \\ a_2'(\eta) &\approx a_2 + (a_1 a_2 - a_1)\eta \\ b_0'(\eta)) &\approx b_0 + (a_1 b_0 - b_1)\eta \\ b_1'(\eta) &\approx b_1 + (a_1 b_1 - 2b_0 - 2b_2)\eta \\ b_2'(\eta)) &\approx b_2 + (a_1 b_2 - b_1)\eta. \end{aligned} \tag{2.6}$$

These new factors do not need division, therefore the VLPF may be calculated using additions and multiplications, as seen in Figure 2.5[49]. Moreover, this understanding does

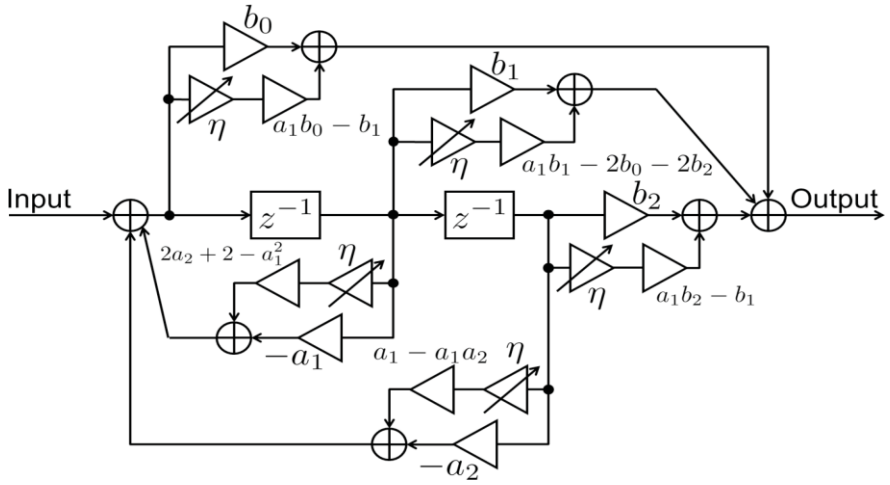

Figure 2.5 Second-order VLPF using frequency transformation and first-order Taylor approximation.

not require recalculation of filter coefficients if η is changed. All multipliers except for η in this block diagram are fixed coefficients.

Although VLPFs based on the Taylor approximation offer an efficient technique of implementation, they have a significant disadvantage in that the range of changeable cutoff frequency is extremely restricted. This constraint is a result of the assumption of $|\eta| \ll 1$, which indicates that the approximation error increases when the cutoff frequency of the VLPFs deviates from that of the prototype filter. Furthermore, if the value of $|\eta|$ is very big, the VLPFs may become unstable. Alternative strategies are given in order to solve these difficulties [23,30]. For the implementation of block diagrams for the prototype filter, all of these techniques use low-sensitivity structures. The replacement $z^{-1} \leftarrow T(z,\eta)$ and Taylor approximation are then applied to these block diagrams, resulting in the appropriate VDFs. Although the approaches presented in [23,30] may be used to restricted classes of transfer functions, the Taylor approximation error becomes less than the typical VDFs based on direct form. This strategy is also used to 2-D VDFs [31].

There are further methods for reducing the Taylor approximation inaccuracy. The technique based on wave digital filters is described in [32]. Although this method requires understanding of analog filter theory, the resulting VDFs are very precise, allowing the variable cutoff frequency to be regulated across a reasonably large range. In [25], the block diagram of the prototype filter is constructed using a state- space representation, and series approximations are employed to minimize the large rise in implementation cost of frequency transformation-based VDFs. The technique of [25] may be used to arbitrary transfer functions and any state-space structures since this method does not need any of the restrictions present in conventional approaches. Moreover, in [11], the VDFs based on the combination of frequency transformation and coefficient decimation are presented, and FPGA implementation and performance assessment demonstrate that the proposed technique achieves very cheap hardware implementation costs.

As stated before, the problem of delay-free loops is crucial to the approximation and implementation of frequency transformation-based VDFs. However, it should be emphasized that this issue does not always occur. In general, this issue occurs when the all-pass function in the frequency transformation contains a constant component that is not zero. This scenario relates to variable bandwidth VDFs. Figure 2.2 demonstrates that the issue of delay-free loops does not occur when the VDFs have a fixed bandwidth.

This paragraph concludes with an overview of the advantages and disadvantages of frequency transformation-based VDFs. The following are the benefits:

- Because the principle of regulating cutoff frequency is based on simple variable transformations, it is straightforward to produce features with changeable parameters.
- If Taylor approximation is not performed, the frequency transformation keeps several relevant aspects about the shape of magnitude responses. For instance, when a prototype low-pass filter is a Butterworth filter with a monotonic and maximally flat magnitude response, the VDFs obtained by performing frequency transformations to this prototype filter likewise have monotonic and maximally flat magnitude responses.
- This advantage enables the design of adaptive band-pass or band-stop filters since

the cost function for adaptive filtering becomes unimodal, resulting in an adaptive algorithm that converges on the globally optimum solution. In the following section, particulars will be explained.

- Compared to the VDFs based on the M-D polynomial approximation, the frequency transformation-based VDFs incur much less computational cost in the filtering process.

Next, the disadvantages are summarized:

- As noted before, if the bandwidth must be changeable in VDFs, the frequency translation results in delay-free loops, an issue that must be addressed effectively.
- To generate VDFs with multiple pass bands or stop bands, such as VBPFs, VBSFs, and variable multiband filters, high-order all-pass functions must be used for frequency transformation. Consequently, the order of VDFs surpasses that of the prototype filter. For instance, the order of the frequency transformation-based VBPFs and VBSFs is doubled compared to the prototype filter's order.
- Because the all-pass functions employed in the frequency transformation are IIR filters, it is not possible to create VDFs with linear phase. Even though the prototype filter is FIR, the frequency changes result in IIR-type VDFs.
- Very few changeable qualities can be realized. Specifically, only VDFs with variable cutoff frequencies may be generated using frequency transformation. In other words, the stop-band attenuation and transition bandwidth cannot be controlled.

2.3.2 VDFs using M-D approximation of filter coefficients

In the realm of VDFs, the M-D polynomial approximation of filter coefficients-based VDFs have been the subject of the many research [6, 10]. One of the key advantages of this method over frequency transformation-based VDFs is the ability to achieve a variety of variable features and changeable cutoff frequencies. As illustrated in Figure 2.6, this method may create VLPFs with variable transition bandwidth and variable stop-band attenuation. In addition, as this method is applicable to both FIR and IIR filters, VDFs may achieve linear-phase characteristics and variable group delay.

The initial stage in obtaining this kind of VDFs is to identify a set of K variable parameters $(\psi_1, \psi_2, \ldots . \psi_k)$ that correspond to the required variable components of frequency characteristics such as cutoff frequency, transition bandwidth, and stop-band attenuation. Spectral parameters are changeable parameters of this kind. Following this stage, the filter coefficients of the required VDFs are represented as M-D polynomials with regard to these variable parameters. As an example, the transfer function of an N-th order VDF with K variable parameters is defined as

$$H(z, \psi_1, \psi_2, \ldots \ldots . \psi_k) = \sum_{n=0}^{N} h_n(\psi_1, \psi_2, \ldots \ldots \psi_k) z^{-n} \tag{2.7}$$

where each filter coefficient $h_n(\psi_1, \psi_2, \ldots . . \psi_k)$ is given in terms of the subsequent M-D polynomial:

$$h_n(\mathcal{Z}, \psi_1, \psi_2, \ldots . \psi_k) = \sum_{m_{\psi_1}=0}^{M_{\psi_1}} \sum_{m_{\psi_2=0}}^{M_{\psi_2}} \ldots \sum_{m_{\psi_k=0}}^{M_{\psi_k}} c_n\,(m_{\psi_1}, m_{\psi_2}, \ldots m_{\psi_k}) {\psi_1}^{m_{\psi_1}} {\psi_2}^{m_{\psi_2}} \ldots {\psi_k}^{m_{\psi_k}} \tag{2.8}$$

Approximating these VDFs requires finding the set of coefficients $\{c_n(m_{\psi_1}, m_{\psi_2}, \ldots m_{\psi_k})\}$ for $0 \leq n \leq N$. Here, $M_{\psi_1}, M_{\psi_2}, \ldots . M_{\psi_k}$ represent the orders of the M-D polynomials that correspond to the variables $\psi_1, \psi_2, \ldots \psi_k$, respectively, the usual method for obtaining the set $\{c_n(m_{\psi_1}, m_{\psi_2}, \ldots m_{\psi_k})\}$, uses a curve-fitting technique to define the intended M-D polynomials and minimizes an error function relative to an ideal characteristic of the desired VDF.

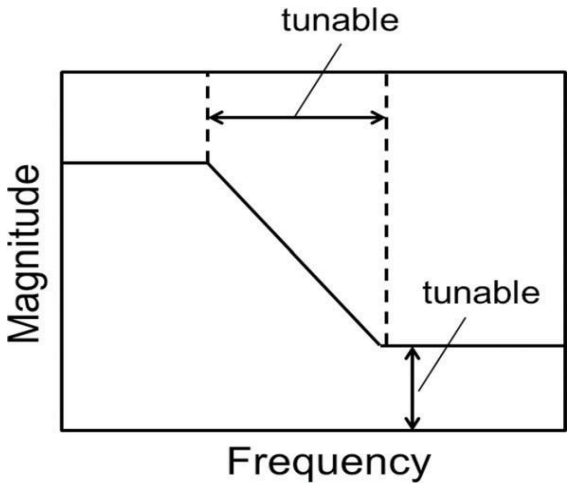

Figure 2.6 This illustration uses a VLPF where the filter coefficients are approximated by an M-D polynomial.

The Farrow structure [33] is often used to implement the VDFs indicated above. To demonstrate this notion, consider a basic VDF with one variable parameter, ψ_1. The expression for this VDF's transfer function is:

$$H(z,\psi_1) = \sum_{n=0}^{N} h_n(\psi_1) z^{-n} = \sum_{n=0}^{N} \sum_{m_{\psi_1}=0}^{M_{\psi_1}} c_n(m_{\psi_1}) {\psi_1}^{m_{\psi_1}} z^{-n} \quad (2.9)$$

it may also be expressed as:

$$H(z,\psi_1) = \sum_{m_{\psi_1}=0}^{M_{\psi_1}} \left(\sum_{n=0}^{N} c_n(m_{\psi_1}) z^{-n}\right) {\psi_1}^{m_{\psi_1}}. \quad (2.10)$$

Consequently, using the following definition:

$$H_{m_{\psi_1}}(z) = \sum_{n=0}^{N} c_n\left(m_{\psi_1}\right) z^{-n}, \quad 0 \le m_{\psi_1} \le M_{\psi_1}, \quad (2.11)$$

the description of the VDF $H(z,\psi_1)$ is now

$$H\left(z,\psi_1\right) = \sum_{m_{\psi_1}=0}^{M_{\psi_1}} H_{m_{\psi_1}}(z) {\psi_1}^{m_{\psi_1}}. \quad (2.12)$$

By using formulation, it is possible to implement $H(z,\psi_1)$ using the Farrow form shown in Figure 2.7 is viewed as the parallel combination of the set of N-th order FIR filters with fixed coefficients and weights ψ_1. Given that these N-th -order FIR Since filters do not contain ψ_1, a recalculation of their coefficients in response to a change in ψ_1 is unnecessary. In this respect, the Farrow structure is appropriate for implementing M-D polynomial approximation-based VDFs.

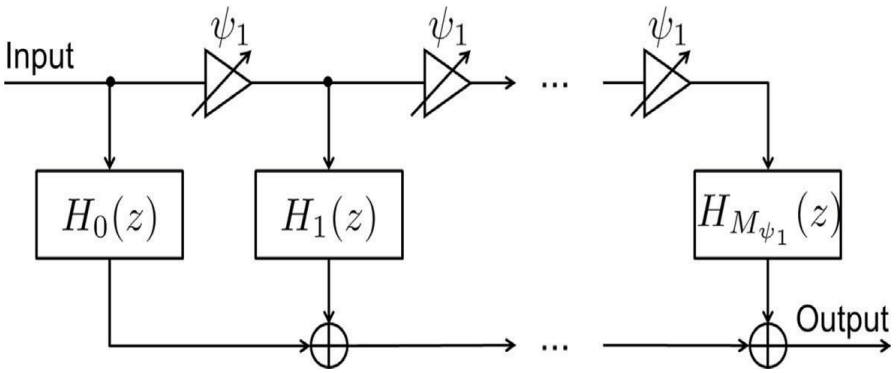

Figure 2.7 Realization of M-D polynomial approximation-based VDF based on the Farrow structure.

Due to the fact that the filter coefficients are characterized by M-D polynomials, M-D polynomial approximation-based VDFs have a high computational cost for filtering. Additionally, this method restricts the scope of changeable attributes. The M-D polynomial approximation imposes this restriction, similar to the Taylor approximation in frequency transformation. In addition, as this method necessitates a number of filters with fixed coefficients, the hardware implementation of these filters may result in an increase in characteristic degradations caused by finite word length effects, such as coefficient sensitivity and round off noise. However, such degradations may be mitigated by using high-precision filter structures, a strategy recently presented in [10]. VDFs with approximation-based structures.

2.3.3 VDFs based on alternative methods

In addition to the two procedures listed above, several more strategies have been given in the literature. By cascading a single sub filter, VDFs with variable bandwidth and no delay-free loops may be constructed at a minimal cost as described in [34]. By adding frequency response masking and the fast filter bank to the design of VDFs, [16, 18] achieves a considerable decrease in implementation costs in comparison to VDFs with the Farrow structure.

In addition, research on VDFs for adaptive filtering has been extensive. Variable notch filters with IIR transfer functions of the second order are a well-known technique in such VDFs. All of these variable notch filters effectively offer changeable features using a simple process that does not need delay-free loops or an increase in computing cost. Other VDFs with an adaptive filter orientation include notch filters with variable attenuation at the notch frequency and comb filters with variable bandwidth and variable attenuation. These subjects will be further upon in the next section.

2.4 VDFs-based adaptive filtering research areas

This section begins with adaptive notch filters (ANFs), a specific instance of adaptive band-stop or band-pass filters. ANFs are the most well-known use of VDFs in adaptive signal processing, and several findings on ANFs have been published since the 1980s. In addition to the ANFs, this section presents many more adaptive filtering-relevant VDFs.

2.4.1 ANF using an all-pass filter

As seen in Figure 2.8[51], an ANF is crucial to the automated identification and suppression of an unknown sinusoid submerged in a wide-band signal, such as white noise. To identify and suppress the sinusoid, the ANF is controlled by an adaptive algorithm such that the notch frequency ω_0 converges to the unknown frequency ω_s of the sinusoid. Consequently, the ANF may be seen as the VDF with a changeable notch frequency, and the value of ω_0 at steady state becomes an approximation of the sinusoid's frequency ω_s.

ANFs are used not only for the detection/suppression of a sinusoid, but also for the estimate of its frequency.

The ANF seen in Figure 2.8 is designed to suppress a sinusoid, but it is also capable of enhancing the sinusoid and suppressing white noise. This is possible by using a peaking filter, also known as a resonator or an inverse notch filter, as an adaptive filter rather than a notch filter. The output of the notch filter may be subtracted from the input signal to improve the sinusoid, such systems, along with those shown in Figure 2.8, are used in a variety of real-world applications, including radar, sonar, telecommunication systems with the suppression of narrowband interference, and howling suppressors in speech processing.

In the next section, we discuss the principles of ANFs, including their problem formulation and the process by which the notch frequency is controlled. As seen in Figure 2.8, ANF problem statements often define the input signal as the sum of a sinusoid and white noise. Consequently, the input signal, denoted $u(n)$, is represented as:

$$u(n) = A\sin(\omega_s n + \phi) + \nu(n) \tag{2.13}$$

where A and ω_s are the amplitude and frequency of the unknown sinusoid, respectively, and is the starting random phase formly distributed in $[0,2\pi]$, $\nu(n)$ is a zero-mean white noise signal that is uncorrelated with ϕ. Let $y(n)$ be the output signal of the ANF based on this configuration.

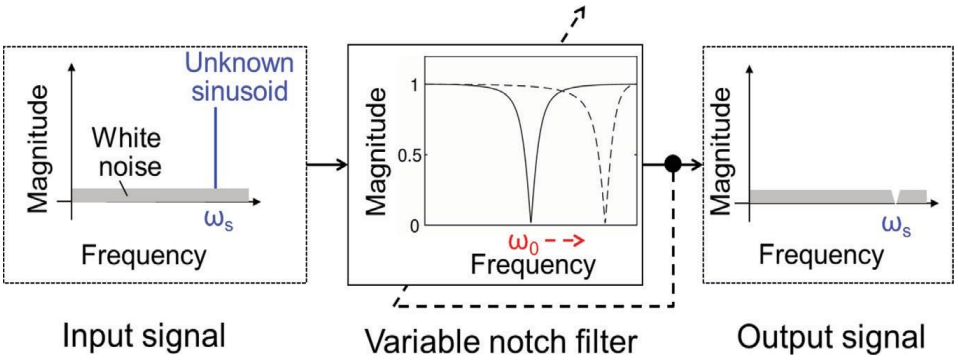

Figure 2.8 ANF for the detection and suppression of sinusoids.

Several approaches exist for describing the transfer function of the notch filter used in adaptive filtering. This chapter focuses on the all-pass filter based on the second order [35]. This notch filter is characterized by the transfer function shown below:

$$H(z,\eta,\xi) = \frac{1}{2}(1 + T(z,\eta,\xi)) \tag{2.14}$$

where $T(z,\eta,\xi)$ is the second-order all-pass filter of the form:

$$T(z,\eta,\xi) = \frac{\eta-(1+\eta)\xi z^{-1}+z^{-2}}{1-(1+\eta)\xi z^{-1}+\eta z^{-2}}. \tag{2.15}$$

Hence Eq. (2.14) is described as

$$H(z,\eta,\xi) = \frac{1+\eta}{2}\frac{1-2\xi z^{-1}+z^{-2}}{1-(1+\eta)\xi z^{-1}+\eta z^{-2}}. \tag{2.16}$$

In this notch filter, the parameter η controls the 3-dB notch width, whereas the parameter controls ξ the notch frequency ω_0. This indicates that the notch filter supplied in this manner has independent control over the notch width and notch frequency. Also of importance is that this notch filter may be viewed as a VDF generated by the frequency transformation [19]: it is evident that this notch filter is created by applying the frequency transformation $z^{-1} \leftarrow T(z,\eta,\xi)$ to the prototype filter of the form:

$$H_p(z) = \frac{1}{2}(1 + z^{-1}). \tag{2.17}$$

Specifically, this notch filter has the same transfer function as the Butterworth band-stop filter of second order [21]. Consequently, this notch filter has a gain of $\omega = 0$ and $\omega = \pi$, and a gain of 0 at ω_0. Moreover, the magnitude response of this notch filter is monotonically reducing $0 < \omega < \omega_0$ and monotonically growing in $\omega_0 < \omega < \pi$.

The ANF block diagram based on this notch filter is shown in Figure 2.9[51]. As previously mentioned, when the ANF reaches steady-state, the sinusoid component of the input $u(n)$ is suppressed at a certain frequency:

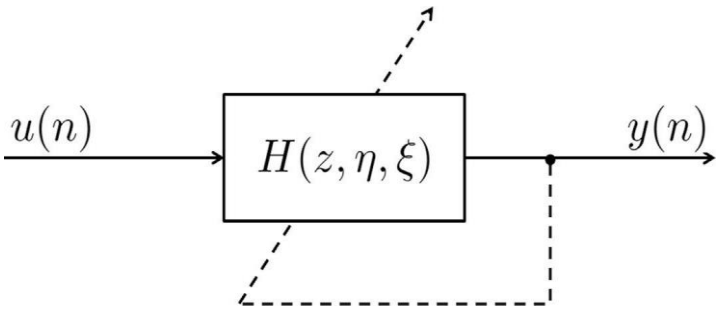

Figure 2.9 ANF based on the second-order all-pass filter.

The signal of output $y(n)$. Here, it is important to note that many adaptive algorithms assume the notch width is constant and only the notch frequency is ω_0 controlled to estimate the sinusoid frequency. Consequently, we concentrate on how to regulate ω_0.

The most common technique for controlling ω_0, is to minimize a cost function using the gradient descent approach. ANFs vary from standard adaptive filters in that the cost function employed in ANFs is the mean square output, or $E[y^2(n)]$. In other words, ANFs typically do not deal with the error signal between a reference signal and the filter output. The cost function $E[y^2(n)]$ must be defined as a function of ω_0, since ANFs regulate ω_0. Moreover, if the input signal is supplied as in Eq. (2.13) and the ANF has monotonic magnitude response, $E[y^2(n)]$ becomes unimodal. Therefore, the gradient descent approach may effectively locate the best notch frequency that minimizes $E[y^2(n)]$ in such a scenario. In reality, the best value of ω_0 corresponds with ω_s when the ANF is based on all passes [36, 37]. Consequently, using the gradient of $E[y^2(n)]$ with regard to ω_0 in an adaptive algorithm enables ω_0 to converge to ω_s, resulting in the detection/suppression of the sinusoid.

2.5 Conclusion

This chapter reviews current research on VDFs, focusing on the approximation issue, the realization challenge, and adaptive filtering applications. Since this chapter has focused on 1-D VDFs with variable magnitude responses, other forms of VDFs, such as M-D VDFs and variable fractional-delay filters, have not been introduced. VDF applications other than adaptive filtering has also been removed for the same reason. Although VDFs have been researched for a considerable amount of time, many elegant discoveries are constantly being offered; hence, VDF research will continue to be an active field of study.

Chapter 3

Frequency transformation for linear state-space systems

3.1 Introduction

One of the well-known strategies for designing analog and digital filters [3, 38] is frequency transformation. This technique, which is based on variable substitution in a transfer function, enables us to easily convert a given prototype low-pass filter into any frequency selective filter, including low-pass filters with different cutoff frequencies, high-pass filters, band-pass filters, and band-stop filters. It is also generally known that converted filters preserve parts of the prototype filter's qualities, such as stability and magnitude response shape. For instance, if a prototype filter is stable and has the Butterworth magnitude response, then the filter is said to have the Butterworth magnitude response, any filter resulting from the frequency transformation is also stable and exhibits the Butterworth feature. Due to this advantageous property, frequency transformation is applicable not only to the construction of filters but also to the real-time adjustment of cutoff frequencies, which may be utilized to the design of variable filters [2] and adaptive notch filtering [19, 20]. Theoretically and practically, the frequency transformation plays a significant role in several current applications of signal processing.

This chapter's objective is to give more insight into the theory of frequency transformation from the perspective of internal filter qualities. In several texts on digital signal processing, frequency transformation is treated only in terms of input-output qualities, i.e. transfer function properties. In other words, few findings concerning the link between frequency transformation and internal attributes have been recorded. According to common knowledge, the internal characteristics of filters are intimately tied to the issue of how to create a filter structure for a particular transfer function, This issue must be carefully examined in order to produce analog filters with a large dynamic range and low sensitivity [39] or digital filters with a high degree of precision in terms of limited

wordlength effects [40, 43]. Consequently, it is beneficial to explore the frequency transformation from the perspective of the internal characteristics and to apply the conclusions to various practical applications.

We utilize the state-space model to explore frequency transformation from the perspective of the internal characteristics of filters. State-space representation is one of the well-known internal descriptions of linear systems, and it also offers a potent instrument for the synthesis of analog/digital filter structures with the aforementioned excellent performance. The outcomes from our talk are twofold. Initially, we demonstrate several advantageous aspects of frequency transformation in terms of the state-space representation. These features are strongly connected to the three components of linear state-space systems listed below: Gramian observability, and the second-order modes. In the characterization of internal characteristics of analog/digital filters and the synthesis of high-performance filter structures, these three factors are recognized to be crucial. Second, we apply this conclusion to the design and synthesis techniques for high-performance analog and digital filters. To be more explicit, we propose easy and unified frameworks for the design and synthesis of analog/digital filters that concurrently achieve the aforementioned high performance and the modification of frequency characteristics. In addition, this finding is extended to variable filters with high-performance structures.

The section is structured as follows. The second section examines the principles of the state-space representation of linear systems, such as analog and digital filters. In Section 3, the classical theory of frequency transformation is introduced. In Section 4, we analyze the frequency transformation using the state-space representation and demonstrate illuminating correlations between the frequency transformation and internal filter features.

3.2 State-space representation, Gramians and second-order modes

In this section, state-space representations of linear systems are introduced. In addition, we present the aforementioned three components on the internal attributes controllability Gramian, observability Gramian, and second-order modes and discuss how they are used to the synthesis of high-performance filter structures. These subjects will be presented, respectively, for digital filters and analog filters.

3.2.1 Representation of digital filters in state space

Take the following state-space equations for a N th-order stable single-input/single-output linear discrete-time system with a single output

:

$$\boldsymbol{x}(n+1) = \boldsymbol{A}\boldsymbol{x}(n) + \boldsymbol{b}u(n)$$
$$y(n) = \boldsymbol{c}\boldsymbol{x}(n) + du(n) \tag{3.1}$$

$u(n)$, $y(n)$ and $\boldsymbol{x}(n) \in \Re^{N\times 1}$ represent the scalar input, scalar output, and state vector, respectively, while $\boldsymbol{A} \in \Re^{N\times N}, \boldsymbol{b} \in \Re^{N\times 1}$, $\boldsymbol{c} \in \Re^{1\times N}$ and $d \in \Re$ are constant coefficients. We will assume that the system is stable, controlled, and observable throughout this whole chapter. If this state-space system represents a digital filter, then each entry of $\boldsymbol{x}(n)$ corresponds to the output of the filter's delay elements. Using the z -transform of the Eq. (3.1), we obtain:

$$z\boldsymbol{X}(z) = \boldsymbol{A}\boldsymbol{X}(z) + \boldsymbol{b}U(z)$$
$$Y(z) = \boldsymbol{c}\boldsymbol{X}(z) + dU(z) \tag{3.2}$$

In terms of $(\boldsymbol{A}, \boldsymbol{b}, \boldsymbol{c}, d)$, the transfer function $H(z)$ is described as

$$H(z) = d + \boldsymbol{c}(z\boldsymbol{I}_N - \boldsymbol{A})^{-1}\boldsymbol{b} \tag{3.3}$$

where $\boldsymbol{I}_N$ denotes the $N \times N$ identity matrix.

It is generally known that the transfer function $H(z)$ is invariant under nonsingular transformation matrices $\boldsymbol{T} \in \Re^{N \times N}$ of the state: if $\boldsymbol{x}(n)$ is converted into $\bar{\boldsymbol{x}}(n) = \boldsymbol{T}^{-1}\boldsymbol{x}(n)$, then the space system $(\boldsymbol{A}, \boldsymbol{b}, \boldsymbol{c}, d)$ is likewise transformed into the set ($\bar{\boldsymbol{A}}, \bar{\boldsymbol{b}}, \bar{\boldsymbol{c}}, \bar{d}$):

$$(\bar{\boldsymbol{A}}, \bar{\boldsymbol{b}}, \bar{\boldsymbol{c}}, \bar{d}) = (\boldsymbol{T}^{-1}\boldsymbol{A}\boldsymbol{T}, \boldsymbol{T}^{-1}\boldsymbol{b}, \boldsymbol{c}\boldsymbol{T}, d). \tag{3.4}$$

It is simple to demonstrate that this new set has the same transfer function as $(\boldsymbol{A}, \boldsymbol{b}, \boldsymbol{c}, d)$. Consequently, several configurations exist for a digital filter with a given transfer function $H(z)$. This nonsingular transformation is referred to as the similarity transformation.

The controllability Gramian, observability Gramian, and second-order modes are introduced next. The solutions $\boldsymbol{K}$ and $\boldsymbol{W}$ to the corresponding Lyapunov equations for the system $(\boldsymbol{A}, \boldsymbol{b}, \boldsymbol{c}, d)$, are known as the controllability Gramian and the observability Gramian, respectively:

$$\begin{aligned} \boldsymbol{K} &= \boldsymbol{A}\boldsymbol{K}\boldsymbol{A}^{\boldsymbol{T}} + \boldsymbol{b}\boldsymbol{b}^{\boldsymbol{T}} \\ \boldsymbol{W} &= \boldsymbol{A}^{\boldsymbol{T}}\boldsymbol{W}\boldsymbol{A} + \boldsymbol{c}^{\boldsymbol{T}}\boldsymbol{c}. \end{aligned} \tag{3.5}$$

Since the system $(\boldsymbol{A}, \boldsymbol{b}, \boldsymbol{c}, d)$ is supposed to be stable, controllable, and observable, the Gramians $\boldsymbol{K}$ and $\boldsymbol{W}$ are symmetric and positive definite, i.e. $\boldsymbol{K} = \boldsymbol{K}^{\boldsymbol{T}} > 0$ and $\boldsymbol{W} = \boldsymbol{W}^{\boldsymbol{T}} > 0$. Consequently, all of the eigenvalues of the matrix product $\boldsymbol{K}\boldsymbol{W}$ are positive. These eigenvalues are denoted as $\theta_1^2, \theta_2^2, \ldots \theta_N^2$ and assume that $\theta_1^2 \geq \theta_2^2, \ldots . \geq \theta_N^2$ and it is assumed that $\theta_1 \geq \theta_2 \ldots . \geq \theta_N$ are referred to as the system's second-order modes. In the literature on control system theory, second-order modes are often referred to as Hankel singular values since $\theta_1, \theta_2, \cdots, \theta_N$ equal the nonzero singular values of the Hankel operator of $H(z)$.

The relationship between the two Gramians and the similarity transformation $\overline{\boldsymbol{x}}(n) = \boldsymbol{T}^{-1}\boldsymbol{x}(n)$ is as follows: The controllability/observability Gramians $(\overline{\boldsymbol{K}}, \overline{\boldsymbol{W}})$ of the system described by Eq. (3.4) are provided by:

$$(\overline{\boldsymbol{K}}, \overline{\boldsymbol{W}}) = (\boldsymbol{T}^{-1}\boldsymbol{K}\boldsymbol{T}^{-T}, \boldsymbol{T}^{T}\boldsymbol{W}\boldsymbol{T}). \tag{3.6}$$

The following relationship explains why the second-order modes are invariant under similarity transformation:

$$\overline{\boldsymbol{K}\boldsymbol{W}} = \boldsymbol{T}^{-1}(\boldsymbol{K}\boldsymbol{W})\boldsymbol{T}. \tag{3.7}$$

Therefore, it follows that Gramians are dependent on system realizations but second-order modes are dependent simply on the transfer function.

In the research on the synthesis of filter structures [40, 43], it is shown that the two Gramians and the second-order modes play crucial roles in the analysis and optimization of filter performance such as roundoff noise and coefficient sensitivity. In other words, given the transfer function of a digital filter, we may build cost functions in terms of the filter's aforementioned performance in terms of the two Gramians ($\boldsymbol{K}, \boldsymbol{W}$), By correctly structuring the two Gramians such that they optimize or sub-optimize the respective cost functions, a high-performance filter structure may be created.

The balanced form is an example of a digital filter construction with superior performance [43, 41]. This structure comprises the two Gramians provided as:

$$\boldsymbol{K} = \boldsymbol{W} = \boldsymbol{\Theta} \tag{3.8}$$

$\boldsymbol{\Theta}$ is the diagonal matrix of the second-order mode:

$$\boldsymbol{\Theta} = diag(\theta_1, \theta_2, \cdots, \theta_N). \tag{3.9}$$

Another illustration is the minimum roundoff noise structure [40, 42], which is comprised of two Gramians satisfying the following relationships:

$$\begin{aligned} \boldsymbol{w} &= (\tfrac{1}{N}\textstyle\sum_{i=1}^{N} \theta_i)^2 \boldsymbol{K} \\ K_{ii} &= 1 \end{aligned} \tag{3.10}$$

K_{ii} corresponds to the i-th diagonal element of $\boldsymbol{K}$.

We conclude by discussing the relevance of second-order modes from two practical perspectives. First, the literature indicates that the second-order modes characterize the optimum values of the aforementioned cost functions. The best performance is thus defined by the second-order modes of a particular transfer function. In the area of balanced

model reduction [44], the second-order modes are proven to give the upper limit for the approximation error between the reduced-order system and the original system.

3.2.2 Representation of analog filters in state space

An *N t*h-order linear continuous-time system (with analog filter) may be represented in state space as follows:

$$\begin{aligned} \frac{d\boldsymbol{x}(t)}{dt} &= \boldsymbol{A}\boldsymbol{x}(t) + \boldsymbol{b}u(t) \\ y(t) &= \boldsymbol{c}\boldsymbol{x}(t) + du(t) \end{aligned} \tag{3.11}$$

where $u(t)$, $y(t)$, and $\boldsymbol{x}(\boldsymbol{t}) \in \Re^{N\times 1}$ are the scalar input, the scalar output, and the state vector of the system, respectively, and $\boldsymbol{A} \in \Re^{N\times N}, \boldsymbol{b} \in \Re^{N\times 1}$, $\boldsymbol{c} \in \Re^{1\times N}$ and $d \in \Re^{1\times 1}$ are constant coefficients. Assume that the system $(\boldsymbol{A}, \boldsymbol{b}, \boldsymbol{c}, d)$ is stable, observable, and controlled. If this system is a continuous-time analog filter with N integrators, then the state vector corresponds to the integrators' output signals.

Laplace transform of the expression (3.11) yields:

$$\begin{aligned} s\boldsymbol{X}(s) &= \boldsymbol{A}\boldsymbol{X}(s) + \boldsymbol{b}U(s) \\ Y(s) &= \boldsymbol{c}\boldsymbol{X}(s) + dU(s), \end{aligned} \tag{3.12}$$

resulting in the subsequent transfer function:

$$H(s) = d + \boldsymbol{c}(s\boldsymbol{I}_N - \boldsymbol{A})^{-\mathbf{1}}\boldsymbol{b}. \tag{3.13}$$

As in the discrete-time example, the transfer function is invariant under similarity transformation: if $x(t)$ is transformed by a nonsingular matrix $\boldsymbol{T} \in \Re^{N\times N}$ into $\boldsymbol{T}^{-1}\boldsymbol{x}(t)$, then the resultant state-space system $(\boldsymbol{T}^{-1}\boldsymbol{A}\boldsymbol{T}, \boldsymbol{T}^{-1}\boldsymbol{b}, \boldsymbol{c}\boldsymbol{T}, d)$ is an equivalent realization to $(\boldsymbol{A}, \boldsymbol{b}, \boldsymbol{c}, d)$ of the transfer function $H(s)$. Consequently, several circuit topologies exist for an analog filter with a given transfer function $H(s)$.

The solutions to the following Lyapunov equations provide the controllability Gramian $\boldsymbol{K}$ and the observability Gramian $\boldsymbol{W}$ of a continuous-time state-space system.:

$$\begin{aligned} \boldsymbol{AK} + \boldsymbol{KA^T} + \boldsymbol{bb^T} &= \mathbf{0}_{N\times N} \\ \boldsymbol{A^T W} + \boldsymbol{W A} + \boldsymbol{c^T c} &= \mathbf{0}_{N\times N} \end{aligned} \tag{3.14}$$

where $\mathbf{0}_{N\times N}$ represents the $N \times N$ zero matrix. Under the condition that $(\boldsymbol{A}, \boldsymbol{b}, \boldsymbol{c}, d)$ is stable, controllable, and observable, the Gramians $\boldsymbol{K}$ and $\boldsymbol{W}$ are proved to be symmetric and positive definite. As in the discrete-time situation, the second-order modes $\theta_1, \theta_2, \cdots, \theta_N$ are found as the positive square roots of $\boldsymbol{KW}$ eigenvalues.

In the case of continuous time, the connection between similarity transformations, Gramians, and second-order modes is identical to that of discrete time. The new Gramians $(\overline{\boldsymbol{K}}, \overline{\boldsymbol{W}})$ of a transformed continuous-time system provided by a similarity transformation $\boldsymbol{T}$ are proven to be $(\boldsymbol{T^{-1}KT^{-T}}, \boldsymbol{T^T WT})$, indicating that the Gramians are dependent on the system's realizations. In contrast, the second-order modes are invariant due to the fact that $\overline{\boldsymbol{KW}} = \boldsymbol{T^{-1}}(\boldsymbol{KW})\boldsymbol{T}$ holds.

As in discrete-time systems, Gramians and second-order modes of continuous-time systems play crucial roles in the synthesis of high-performance filter architectures [39]. You may achieve a high-performance structure by optimizing or sub-optimizing a predefined cost function in terms of the controllability and observability Gramians. This cost function may be interpreted as a measure of the dynamic range and sensitivity of an analog filter. The best values of such cost functions are also determined by the second-order modes.

3.3 Frequency transformation

3.3.1 Digital filter frequency transformation

Oppenheim [45] and Constantinides [3] provide examples of frequency transformations of digital filters. Oppenheim's research is applied to finite impulse response (FIR) transfer functions, whereas Constantinides' research is used to Infinite

Impulse Response (IIR) transfer functions. The frequency transformation of digital filters is limited to the work of Constantinides in this chapter.

Let $H(z)$ be the transfer function of a digital low-pass filter of order N-th. The discrete-time frequency transformation is described as:

$$H(F(z)) = H(z)\,|_{z^{-1}\,\to 1/F(z)} \tag{3.15}$$

resulting in a brand-new composite transfer function $H(F(z))$. For this transformation, the function $1/F(z)$ is defined as M-th order stable all-pass function of the type:

$$\begin{aligned} \frac{1}{F(z)} &= \pm z^{-M}\,\frac{G(z^{-1})}{G(z)} \\ G(z) &= 1 + \textstyle\sum_{k=1}^{M} g_k z^{-k}. \end{aligned} \tag{3.16}$$

The well-known common frequency transformations use the four following all-pass functions [4]:

$$\begin{aligned} \frac{1}{F_{LP(z)}} &= \frac{z^{-1}-\xi}{1-\xi z^{-1}} \\ \frac{1}{F_{HP(z)}} &= -\frac{z^{-1}+\xi}{1+\xi z^{-1}} \\ \frac{1}{F_{BP(z)}} &= -\frac{z^{-2}-\frac{2\xi\eta}{\eta+1}z^{-1}+\frac{\eta-1}{\eta+1}}{1-\frac{2\xi\eta}{\eta+1}z^{-1}+\frac{\eta-1}{\eta+1}z^{-2}} \\ \frac{1}{F_{BS(z)}} &= \frac{z^{-2}-\frac{2\xi\eta}{1+\eta}z^{-1}+\frac{1-\eta}{1+\eta}}{1-\frac{2\xi\eta}{1+\eta}z^{-1}+\frac{1-\eta}{1+\eta}z^{-2}} \end{aligned} \tag{3.17}$$

corresponding to the low-pass-low-pass (LP-LP), low-pass-high-pass (LP-HP), low-pass-band-pass (LP-BP), and low-pass-band-stop (LP-BS) transformations, respectively. The cutoff frequencies of the modified filters are determined by the parameters ξ and η. On the block diagram of a digital filter, frequency transformation signifies that every delay element z^{-1} in $H(z)$ is replaced with an all-pass filter $1/F(z)$.

3.3.2 Frequency transformation using analog filters

Let $H(s)$ represent the transfer function of an analog low-pass filter of order N. The following variable substitution describes the frequency transformation of analog filters: [38]:

$$H\big(F(s)\big) = H(s)|_{s^{-1}\leftarrow 1/F(s)}. \tag{3.18}$$

Consequently, the frequency transformation produces a new composite transfer function $H\big(F(s)\big)$ from the prototype transfer function $H(s)$. In general, the prototype low-pass filter has a cutoff frequency of 1 rad/s. From a circuit perspective, the substitution $s^{-1} \leftarrow 1/F(s)$ signifies that each integrator 1/s in the prototype filter $H(s)$ is substituted with another system whose transfer function is $1/F(s)$.

The transformation function $1/F(s)$ is defined as the Foster reactance function [38] shown below:

$$\frac{1}{F(s)} = \frac{Z(s)}{P(s)} = G\,\frac{(s^2+\omega_{z1}^2)+(s^2+\omega_{z2}^2)+(s^2+\omega_{z3}^2)\ldots\ldots}{s(s^2+\omega_{P1}^2)(s^2+\omega_{P2}^2)(s^2+\omega_{P3}^2)\ldots\ldots} \tag{3.19}$$

where $G > 0$ and $0 \le \omega_{z1} < \omega_{P1} < \omega_{z2} < \omega_{P2} < \omega_{z3} < \omega_{P3} < \cdots$. The Foster reactance functions are defined so that the degree of difference between $p(s)$ and $z(s)$ is 1, i.e. $|\,deg\,p(s) - deg\,z(s)| = 1$.. In the case of the well-known typical LP-LP, LP-HP, LP-BP, and LP-BS transformations, the corresponding reactance functions are given as [4]:

$$\begin{aligned}
\frac{1}{F_{LP(s)}} &= \frac{G}{s} \\
\frac{1}{F_{HP(s)}} &= Gs \\
\frac{1}{F_{BP(s)}} &= \frac{Gs}{s^2+\omega_{p1}^2} \\
\frac{1}{F_{BS(S)}} &= \frac{G(s^2+\omega_{z1}^2)}{s}.
\end{aligned} \tag{3.20}$$

Cutoff frequencies of modified filters are determined by the parameters $G, \omega_p,$ and ω_s.

It is vital to note that the Foster reactance functions fall into two distinct categories: suitable reactance functions and improper reactance functions. $1/F_{LP(s)}$ and $1/F_{BP(s)}$ correspond to strictly correct reactance functions in the usual frequency transformations of Eq.(3.20), while $1/F_{HP(s)}$ and $1/F_{BS(s)}$ are improper reactance functions.

3.4 Analysis of frequency transformation in state space

This section examines frequency transformation from the perspective of internal characteristics. In other words, we demonstrate a multitude of intriguing outcomes of the frequency transformation in terms of the state-space representation.

This study stems from the work of Mullis and Roberts [46], in which they proposed a simple state-space formulation of frequency transformation for digital filters and demonstrated an essential characteristic of the second-order modes, namely that they are invariant under frequency transformation. In addition, they discussed design and synthesis implications of these discoveries for high-performance digital filters.

This chapter begins with an introduction to this work, followed by a discussion of the link between frequency transformation and state-space representation of discrete-time systems. Additionally, we give comparable findings for continuous-time systems.

3.4.1 State-space formulation of frequency transformation for digital filter filters and invariance of second-order modes

The first explicit state-space formulation of frequency transformation was published by Mullis and Roberts [46] as follows. $(\boldsymbol{A}, \boldsymbol{b}, \boldsymbol{c}, d)$ is a state-space representation of the prototype filter $H(z)$. The transfer function $H(F(z))$ obtained by the frequency transformation od Eq.(3.15) with a M-th order all-pass function $1/F(z)$ may therefore be expressed clearly as follows:

$$H(F(z)) = D + \boldsymbol{C}(z\boldsymbol{I}_{MN} - \boldsymbol{A})^{-1}\boldsymbol{B} \tag{3.21}$$

Using the coefficients shown below:

$$\begin{aligned} \boldsymbol{A} &= \boldsymbol{I}_N \otimes \boldsymbol{\alpha} + [\boldsymbol{A}(\boldsymbol{I}_N - \delta\boldsymbol{A})^{-1}] \otimes (\boldsymbol{\beta\gamma}) \\ \boldsymbol{B} &= [(\boldsymbol{I}_N - \delta\boldsymbol{A})^{-1}\boldsymbol{b}] \otimes \boldsymbol{\beta} \\ \boldsymbol{C} &= [\boldsymbol{c}(\boldsymbol{I}_N - \delta\boldsymbol{A})^{-1}] \otimes \boldsymbol{\gamma} \\ D &= d + \delta\boldsymbol{c}(\boldsymbol{I}_N - \delta\boldsymbol{A})^{-1}\boldsymbol{b} \end{aligned} \tag{3.22}$$

where $(\boldsymbol{\alpha}, \boldsymbol{\beta}, \boldsymbol{\gamma}, \delta)$ is a state-space representation of $1/F(z)$, and $\otimes$ is the Kronecker product for matrices.

The relevance of the description provided by Eq.(3.22) resides in the fact that, using this description, it is simple to perform frequency transformations on a state-space structure and a transfer function. Additionally, notice that this explanation contains no delay-free loops.

In add to the state-space model shown above, Mullis and Roberts detailed the Gramians and second-order modes of the transformed system $(\boldsymbol{\mathcal{A}}, \boldsymbol{\mathcal{B}}, \boldsymbol{\mathcal{C}}, \mathcal{D})$. The two Gramians, indicated by the symbols $\boldsymbol{k}$ and $\boldsymbol{w}$, are presented as follows:

$$\begin{aligned} \boldsymbol{\mathcal{K}} &= \boldsymbol{K} \otimes \boldsymbol{Q} \\ \boldsymbol{\mathcal{W}} &= \boldsymbol{W} \otimes \boldsymbol{Q^{-1}} \end{aligned} \tag{3.23}$$

where $\boldsymbol{Q}$ is the controllability Gramian for the all-pass system $(\boldsymbol{\alpha}, \boldsymbol{\beta}, \boldsymbol{\gamma}, \delta)$. We may deduce readily from this relationship:

$$\boldsymbol{\mathcal{K}\mathcal{W}} = (\boldsymbol{KW}) \otimes \boldsymbol{I}_M \tag{3.24}$$

Consequently, the eigenvalues of the matrix product $\boldsymbol{\mathcal{K}\mathcal{W}}$ are identical to those of $\boldsymbol{KW}$ with multiplicity M. This demonstrates that the second-order modes of converted filters are identical to those of a particular prototype filter. Therefore, the modes of second-order digital filters are invariant under frequency transformation.

The practical value of this characteristic of invariance is addressed below. As indicated in Section 2, second-order modes generate optimum cost function values with regard to word length effects. Using the knowledge that the least roundoff noise is defined by second-order modes, [46] demonstrates that the minimum value of the roundoff noise of digital filters is independent of the frequency transformation-controlled filter features. Similarly, the upper limit of the approximation error owing to the balanced model reduction is invariant under frequency transformation.

In addition, in the case of LP-LP transformation, [46] gives the unique state-space-based frequency transformation that preserves optimum realizations. This particular transformation is provided by:

$$\begin{aligned}
\boldsymbol{\mathcal{A}} &= (\xi \boldsymbol{I}_N + \boldsymbol{A})(\boldsymbol{I}_N + \xi \boldsymbol{A})^{-1} \\
\boldsymbol{\mathcal{B}} &= \sqrt{1-\xi^2}(\boldsymbol{I}_N + \xi \boldsymbol{A})^{-1}\boldsymbol{b} \\
\boldsymbol{\mathcal{C}} &= \sqrt{1-\xi^2}\boldsymbol{c}(\boldsymbol{I}_N + \xi \boldsymbol{A})^{-1} \\
\mathcal{D} &= d - \xi \boldsymbol{c}(\boldsymbol{I}_N + \xi \boldsymbol{A})^{-1}\boldsymbol{b}.
\end{aligned} \tag{3.25}$$

By setting the prototype state-space filter $(\boldsymbol{A}, \boldsymbol{b}, \boldsymbol{c}, d)$ to its ideal realization and using Eq.(3.25), arbitrary low-pass filters with the same optimal realization as the prototype filter may be obtained.

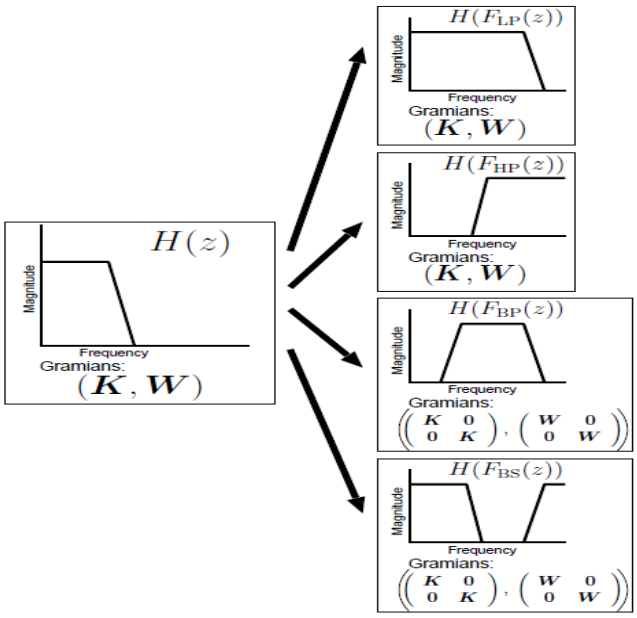

Figure 3.1 Gramian-preserving frequency transformation.

3.4.2 Gramian-preserving frequency transformation in digital filtering

Here, we focus on the controllability and observability of Gramians and present a novel state-space formulation of frequency transformation that maintains the invariance of these Gramians. The Gramian-preserving frequency transformation is a new state-space-based frequency transformation that contains the formulation of Eq.(3.25) as a specific instance.

Before presenting the mathematical definition of the Gramian-preserving frequency transformation, we explain its relationship to the design and synthesis of digital filters. Figure 3.1 provides straightforward examples of the design/synthesis of low-pass, high-pass, band-pass, and band-stop filters. Assume here that we are given a prototype low-pass filter with the transfer function $H(z)$ shown on the left side of this figure. Moreover, let the controllability and observability Gramians of this filter prototype be $\boldsymbol{K}$ and $\boldsymbol{W}$, respectively. Then, by applying the Gramian-preserving frequency transformation to this prototype filter, we can turn it into various arbitrary low-pass, high-pass, band-pass, and band-stop filters with the same controllability/observability Gramians as the prototype filter.

The Gramian-preserving frequency transformation is a particularly effective method for simultaneously designing and synthesizing high-performance digital fitlers. In other words, if we prepare the structure of a given prototype low-pass filter as a high-performance structure, such as the balanced form and the minimum roundoff noise form, the Gramian-preserving frequency transformation allows us to obtain other types of filters with the same high-performance structure, this is also true for analog filters.

The mathematical description of the Gramian-preserving frequency transformation is now presented. Given a state-space digital filter prototype $(\boldsymbol{A}, \boldsymbol{b}, \boldsymbol{c}, d)$ with the transfer function $H(z)$ and a M-th order all-pass function $1/F(z)$, the following description offers the Gramian-preserving frequency transformation to construct the composite transfer function $H(F(z))$[47]:

$$\widetilde{\boldsymbol{\mathcal{A}}} = \widetilde{\boldsymbol{\alpha}} \otimes \boldsymbol{I}_N + (\widetilde{\boldsymbol{\beta}}\widetilde{\boldsymbol{\gamma}}) \otimes \left[\boldsymbol{A}(\boldsymbol{I}_N - \tilde{\delta}\boldsymbol{A})^{-1}\right]$$

$$\widetilde{\boldsymbol{\mathcal{B}}} = \widetilde{\boldsymbol{\beta}} \otimes [(\boldsymbol{I}_N - \tilde{\delta}\boldsymbol{A})^{-1}\boldsymbol{b}]$$

$$\widetilde{\boldsymbol{C}} = \widetilde{\boldsymbol{\gamma}} \otimes [\boldsymbol{c}\left(\boldsymbol{I}_N - \tilde{\delta}\boldsymbol{A}\right)^{-1} \tag{3.26}$$
$$\widetilde{D} = d + \tilde{\delta}\boldsymbol{c}\left(\boldsymbol{I}_N - \tilde{\delta}\boldsymbol{A}\right)^{-1}\boldsymbol{b}$$

and that $(\widetilde{\boldsymbol{\alpha}}, \widetilde{\boldsymbol{\beta}}, \widetilde{\boldsymbol{\gamma}}, \tilde{\delta})$ is a state-space representation of $1/F(z)$ and the controllability/observability Gramians are equal to the identity matrix, i.e.

$$\widetilde{\boldsymbol{\alpha}}\widetilde{\boldsymbol{\alpha}}^{\boldsymbol{T}} + \widetilde{\boldsymbol{\beta}}\widetilde{\boldsymbol{\beta}}^{\boldsymbol{T}} = \widetilde{\boldsymbol{\alpha}}^{\boldsymbol{T}}\widetilde{\boldsymbol{\alpha}} + \widetilde{\boldsymbol{\gamma}}^{\boldsymbol{T}}\widetilde{\boldsymbol{\gamma}} = \boldsymbol{I}_M. \tag{3.27}$$

This relationship indicates that the set $(\widetilde{\boldsymbol{\alpha}}, \widetilde{\boldsymbol{\beta}}, \widetilde{\boldsymbol{\gamma}}, \tilde{\delta})$ is a balanced form. Observe that such a set always exists if $1/F(z)$ is stable.

Now we will examine the mathematical formulation of the Gramians of ($\widetilde{\boldsymbol{A}}$, $\widetilde{\boldsymbol{B}}$, $\widetilde{\boldsymbol{C}}$, $\widetilde{D}$), which are denoted by $\widetilde{\boldsymbol{\mathcal{K}}}$ and $\widetilde{\boldsymbol{\mathcal{W}}}$, respectively. They are presented as follows in terms of the Gramians of the prototype filter:

$$\widetilde{\boldsymbol{\mathcal{K}}} = \boldsymbol{I}_M \otimes \boldsymbol{k}$$
$$\widetilde{\boldsymbol{\mathcal{W}}} = \boldsymbol{I}_M \otimes \boldsymbol{w} \tag{3.28}$$

Thus, $\widetilde{\boldsymbol{\mathcal{K}}}$ and $\widetilde{\boldsymbol{\mathcal{W}}}$ form block diagonal matrices with *M* diagonal blocks that are all identical to $\boldsymbol{k}$ and $\boldsymbol{W}$. As indicated above, $\widetilde{\boldsymbol{\mathcal{K}}}$ and $\widetilde{\boldsymbol{\mathcal{W}}}$ respectively become the same as $\boldsymbol{k}$ and $\boldsymbol{W}$ as multiplicity *M*. Therefore Eq.(3.26), the Gramians are preserved via frequency transformation.

The Gramian-preserving frequency transformation is next discussed from a realization standpoint. First, we see from Eq.(3.27), that in order to implement the Gramian-preserving frequency transformation, the structure of the all-pass filter $1/F(z)$, must be constructed so that its state-space representation assumes a balanced form. Although it is known that the formulation of the balanced form for a given transfer function is not unique, we offered a beneficial approach: Given an all-pass transfer function $1/F(z)$, the normalized lattice structure converts into a balanced form, enabling the Gramian-preserving frequency transformation to be implemented. This is the result of seeing that $1/F(z)$is all-pass. Recall that the frequency transformation of digital filters

necessitates the replacement of each delay element in a prototype filter with an all-pass filter (and the subsequent deletion of any delay-free loops).

In light of this, we may deduce that the Gramian-preserving frequency transformation is read as the replacement of each delay element in the prototype filter with a normalized lattice structure all-pass filter. Figure 3.2 [4] depicts this design. Given a state-space prototype filter as shown in Figure 3.2(a), we perform the aforementioned replacement and receive a changed state-space prototype filter as shown in Figure 3.2(b). The all-pass filter incorporated in this construction is comprised of M lattice sections $\Phi_1, \cdots, \Phi_M$, with each section Φ_i shown in Figure 3.2(c). The variable $\hat{\xi}_i$ signifies the i-th lattice coefficient for $1/F(z)$, when ξ_i for $1 \leq i \leq M$, and $\hat{\xi}_i = \sqrt{1-\xi^2}$.

Finally, the mathematical formulation of the Gramian-preserving frequency transformation based on the normalized lattice structure is presented. The normalized lattice structure of $1/F(z)$ may be represented in state space as follows [48]:

$$\tilde{\boldsymbol{\alpha}} = \begin{pmatrix} -\hat{\xi}_1 & -\hat{\xi}_1\hat{\xi}_2 & -\hat{\xi}_1\hat{\xi}_2\hat{\xi}_3 \cdots & -\hat{\xi}_1\hat{\xi}_2\hat{\xi}_3 \cdots & \hat{\xi}_{M-3}\hat{\xi}_{M-2} & -\hat{\xi}_1\hat{\xi}_2\hat{\xi}_3 \cdots & \hat{\xi}_{M-2}\hat{\xi}_{M-1} & -\hat{\xi}_1\hat{\xi}_2\hat{\xi}_3 \cdots & \hat{\xi}_{M-1}\hat{\xi}_M \\ \hat{\xi}_1 & -\hat{\xi}_1\hat{\xi}_2 & -\hat{\xi}_1\hat{\xi}_2\hat{\xi}_3 \cdots & -\hat{\xi}_1\hat{\xi}_2\hat{\xi}_3 \cdots & \hat{\xi}_{M-3}\hat{\xi}_{M-2} & -\hat{\xi}_1\hat{\xi}_2\hat{\xi}_3 \cdots & \hat{\xi}_{M-2}\hat{\xi}_{M-1} & -\hat{\xi}_1\hat{\xi}_2\hat{\xi}_3 \cdots & \hat{\xi}_{M-1}\hat{\xi}_M \\ \cdot & \cdot & \cdot & \cdot & \cdot & \cdot & \cdot & \cdot & \cdot \\ \cdot & \cdot & \cdot & \cdot & \cdot & \cdot & \cdot & \cdot & \cdot \\ \cdot & \cdot & \cdot & \cdot & \cdot & \cdot & \cdot & \cdot & \cdot \\ 0 & 0 & 0 & \cdots & 0 & & \hat{\xi}_{M-1} & \hat{\xi}_{M-1}\hat{\xi}_M & \end{pmatrix}$$

$$\tilde{\boldsymbol{\beta}} = \begin{pmatrix} \hat{\xi}_1\hat{\xi}_2\hat{\xi}_3 \cdots & \hat{\xi}_{M-2}\hat{\xi}_{M-1} \\ \hat{\xi}_1\hat{\xi}_2\hat{\xi}_3 \cdots & \hat{\xi}_{M-1}\hat{\xi}_M \\ \hat{\xi}_2\hat{\xi}_3 \cdots & \hat{\xi}_{M-1}\hat{\xi}_M \\ & \cdot \\ & \cdot \\ \hat{\xi}_{M-2}\hat{\xi}_{M-1}\hat{\xi}_M & \\ \hat{\xi}_{M-1}\hat{\xi}_M & \end{pmatrix}$$

$$\tilde{\boldsymbol{\gamma}} = \begin{pmatrix} 0 & 0 & 0 \dots \dots 0 \pm \hat{\xi}_M \end{pmatrix} \tag{3.29}$$

$$\tilde{\delta} = \pm\hat{\xi}_M.$$

Therefore, the Gramian-preserving frequency change is carried out by substituting Eq.(3.29) with Eq.(3.26). Note that the state-space representation $(\widetilde{\boldsymbol{\mathcal{A}}}, \widetilde{\boldsymbol{\mathcal{B}}}, \widetilde{\boldsymbol{\mathcal{C}}}, \widetilde{\mathcal{D}})$. produced in this manner becomes sparse because and contain numerous zero entries n $\widetilde{\boldsymbol{\alpha}}$ and $\widetilde{\boldsymbol{\gamma}}$. To be exact, the set $(\widetilde{\boldsymbol{\mathcal{A}}}, \widetilde{\boldsymbol{\mathcal{B}}}, \widetilde{\boldsymbol{\mathcal{C}}}, \widetilde{\mathcal{D}})$ has in total $(M-1)N(MN-M/2)$ zero entries. Consequently, this state-space filter is well suited for implementation.

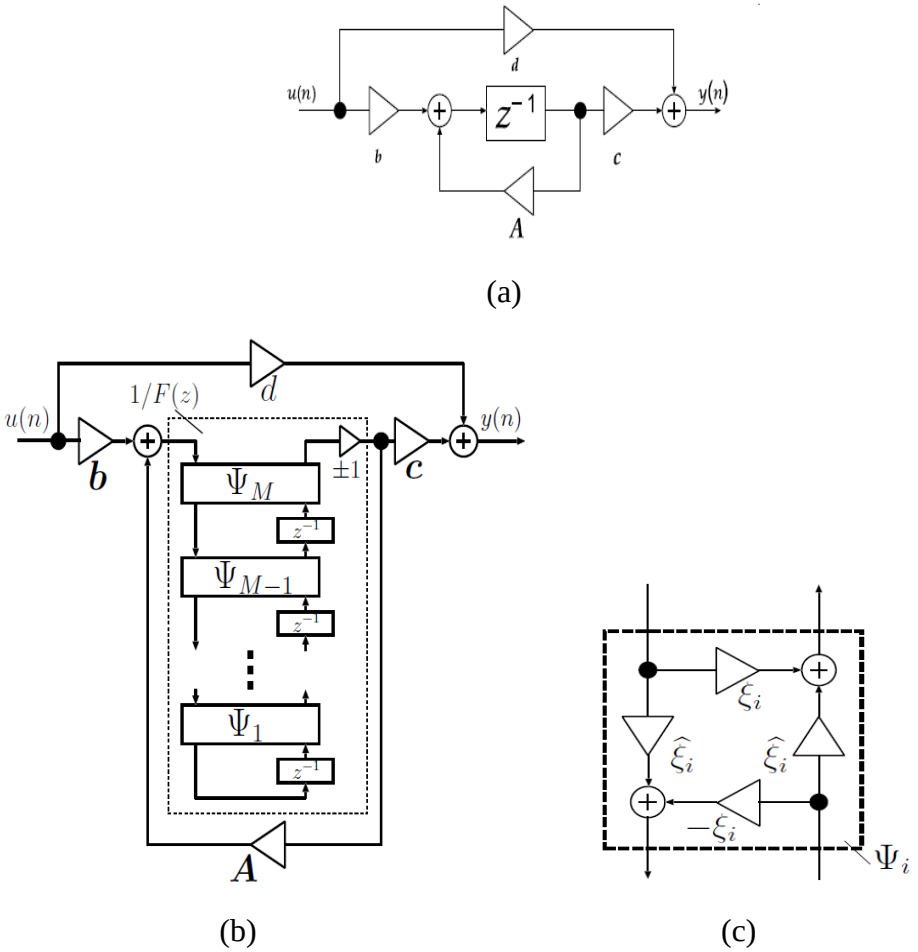

Figure 3.2 Gramian-preserving frequency transformation (a) prototype state-space filter, (b) trnansformed state-space filter, and (c) normalized lattice section Ψ_i.

3.5 Conclusion

In this chapter, we presented insightful and practical discoveries about the classical frequency transformation of analog and digital filters. While the majority of known results on frequency transformation are described in terms of transfer functions, the results presented in this chapter are based on the state-space representation, which has revealed many useful properties regarding the performance of filters whose internal properties and input-output relationship dominate. For the design and synthesis of high-performance filters, the Gramian-preserving frequency transformation is very interesting.

Chapter 4

Series approximations for variable state-space digital filters

4.1 Introduction

Let $H_p(z)$ represent the transfer function of a low-pass filter prototype with the N-th order IIR. The required VDF of the transfer function $H(z)$ is derived from $H_p(z)$ using the frequency transformation shown below.[3]

$$H(z) = H_p(z)\big|_{z^{-1}\leftarrow T(z)} \tag{4.1}$$

Where $T(z)$ is an all-pass transfer function, the selection of $T(z)$ is contingent upon the specification of VDFs, i.e. VLPFs, VHPFs, VBPFs, and VBSFs.

This section examines the design of VLPFs. Let $H_{LP}(z,\eta)$ be the transfer function of the desired VLPF, where η is the parameter for tuning the cutoff frequency (i.e., the bandwidth) of the VLPF. Then, $H_{LP}(z,\eta)$ is derived by the subsequent LP-LP transformation using the first-order all-pass transfer function $T_{LP}(z,\eta)$:

$$\begin{aligned} H_{LP}(z,\eta) &= H_p(z)\big|_{z^{-1}\leftarrow T_{LP}(z,\eta)} \\ T_{LP}(z,\eta) &= \frac{z^{-1}-\eta}{1-\eta z^{-1}} \end{aligned} \tag{4.2}$$

Note that η must meet $|\eta| < 1$ in order to assure the stability of $H_{LP}(z,\eta)$. If $\eta > 0$, the bandwidth of $H_{LP}(z,\eta)$ is smaller than that of $H_p(z)$, and it gets larger if $\eta < 0$. Figure 2.1 depicts a VLPFs that has been adjusted in this manner.

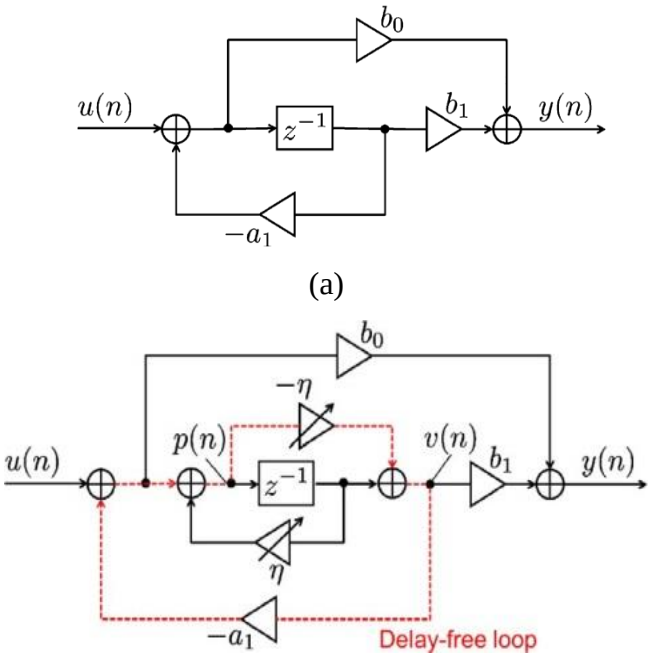

Figure 4.1 Problem with straight LP-LP transformation usage: (a) first-order filter prototype and (b) transformed filter with delay-free loop.

4.1.1 Problem with straight LP-LP transformation usage

From a practical standpoint, it is difficult to directly apply the LP-LP transformation described above. Consider the following example of a first-order prototype filter:

$$H_p(z) = \frac{b_0 + b_1 z^{-1}}{1 + a_1 z^{-1}} \tag{4.3}$$

The structure is shown in Figure 4.1[25] by the direct form II (a). Changing the delay component of this filter with $T_{LP}(z, \eta)$ generates the new filter structure, as shown in Figure 4.1(b). Using $v(n)$ and $p(n)$ as in Figure 4.1(b), we obtain

$$\begin{aligned} v(n) &= -\eta p(n) + p(n-1) \\ p(n) &= \eta p(n-1) - a_1 v(n) + u(n) \\ y(n) &= b_1 v(n) + b_0[-a_1 v(n) + u(n)] \end{aligned} \tag{4.4}$$

Where $u(n)$ and $y(n)$ represent the filter's input and output, respectively. It follows from this connection that

$$v(n) = -\eta[\eta p(n-1) - a_1 v(n) + u(n)] + p(n-1) \quad (4.5)$$

Since the term $v(n)$ appears on the right-hand side of Eq.(4.5), it is now clear that $v(n)$ cannot be computed. Consequently, the delay-free loops produce an unrealizable structure. It is common knowledge that delay-free loops can be prevented by manipulating difference equations. In the above example. Eq.(4.5) is rewritten to

$$v(n) = \frac{1}{1-\eta a1}\,[(1-\eta^2)p(n-1) - \eta u(n)] \quad (4.6)$$

Consequently, $v(n)$ may be omitted, resulting in the following set of differential equations without delay-free loops:

$$\begin{aligned} p(n) &= \frac{\eta - a_1}{1-\eta a_1} p(n-1) + \frac{1}{1-\eta a_1} u(n) \\ y(n) &= (b_0 - b_1\eta)p(n) + (b_1 - b_0\eta)p(n-1) \end{aligned} \quad (4.7)$$

Although delay-free loops may be deleted in this manner, the process is difficult and time-consuming. For high-order filters or highly complex structures, such as lattice structures, great attention must be paid to effectively executing manipulations of difference equations. Moreover, it is evident from Eq.(4.7) that the deletion of delay-free loops often involves expensive hardware-intensive division operations.

Recalculating the transfer function $H_{LP}(z,\eta)$ coefficients is another method for avoiding delay-free loops in the LP-LP transformation. In the case of those mentioned above, first-order, applying the LP-LP transformation to Eq.(4.3) and rearranging the numerator and denominator of $H_{LP}(z,\eta)$ results in the expression:

$$H_{LP}(z,\eta) = \frac{\frac{b_0 - b_1\eta}{1-a_1\eta} + \frac{b_1 - b_0\eta}{1-a_1\eta} z^{-1}}{1 + \frac{a_1 - \eta}{1-a_1\eta} z^{-1}} \quad (4.8)$$

Therefore, by recalculating each coefficient in Eq.(4.8) according to the update, the VLPF may be implemented without delay-free loops. In the case of higher-order filters, both coefficients in Eq.(4.7) and Eq.(4.8) include division operations and become much more difficult. For instance, when $H_p(z)$ is the IIR filter of second order shown below:

$$H_P(z) = \frac{b_0+b_1z^{-1}+b_2z^{-2}}{1+a_1z^{-1}+a_2z^{-2}} \tag{4.9}$$

The transfer function of $H_{LP}(z,\eta)$ becomes

$$H_{LP}(z,\eta)= \frac{\frac{b_0-b_1\eta+b_2\eta^2}{1-a_1\eta+a_2\eta^2}+\frac{-2b_0\eta+b_1(1+\eta^2)-2b_2\eta}{1-a_1\eta+a_2\eta^2}z^{-1}+\frac{b_0\eta^2-b_1\eta+b_2}{1-a_1\eta+a_2\eta^2}z^{-2}}{1+\frac{-2\eta+a_1(1+\eta^2)-2a_2\eta}{1-a_1\eta+a_2\eta^2}z^{-1}+\frac{\eta^2-a_1\eta+a_2}{1-a_1\eta+a_2\eta^2}z^{-2}} \tag{4.10}$$

Which coefficients are more complex than the coefficients in the first-order case. For these reasons, the use of the LP-LP transformation directly is impractical for realization.

4.1.2 VLPFs approximated using the Taylor series

In [30], an effective solution to the above disadvantage is presented. Under the assumption that $|\eta| \ll 1$, this technique applies the first-order Taylor series approximation for to each filter coefficient in $H_{LP}(z,\eta)$. This method simplifies the $H_{LP}(z,\eta)$ filter coefficients that do not involve division operations. Regarding the second-order VLPF, as in Eq.(4.10). Applying the Taylor series approximation of the first order produces:

$$\begin{aligned} H_{LP}(z,\eta) &\cong \overline{H}_{LP}(z,\eta) \\ &= \frac{\bar{b}_0(\eta)+\bar{b}_1(\eta)z^{-1}+\bar{b}_2(\eta)z^{-2}}{1+\bar{a}_1(\eta)z^{-1}+\bar{a}_2(\eta)z^{-2}} \end{aligned} \tag{4.11}$$

where

$$\begin{aligned} \bar{a}_1(\eta) &= a_1 + ({a_1}^2 - 2 - 2a_2)\eta \\ \bar{a}_2(\eta) &= a_2 + (a_1a_2 - a_1)\eta \\ \bar{b}_0(\eta) &= b_0 + (a_1b_0 - b_1)\eta \end{aligned}$$

$$\bar{b}_1(\eta) = b_1 + (a_1 b_1 - 2b_0 - 2b_2)\eta \qquad (4.12)$$
$$\bar{b}_2(\eta) = b_2 + (a_1 b_2 - b_1)\eta.$$

Therefore, this VLPF can be readily built with only the adder and multipliers. Observe that using too large of $|\eta|$ can severely degrade the frequency response or violate stability.

4.2 Proposed method

The suggested technique is a state-space variant of the previously described method. The state-space technique is preferred over the transfer function approach for two reasons. The state-space technique provides a more precise approximation in the VDF design, which is the primary reason. As previously stated, the transfer function technique employs the Taylor series approximation, and in most circumstances, this approximation must depend on the first-order approximation since considering more than second-order terms in valves would need an overly complex mathematical formulation. In contrast, the technique provided in this section can readily handle higher-order approximation in a simple algebraic formulation, resulting in a more precise VDF design than the transfer function approach. The second reason is that the state-space technique is a potent instrument that produces great accuracy regarding limited word length effects. As well known, the behaviour of finite word length effects, such as the coefficient quantization error and the round-off error, is highly dependent on the filter structures used. In other words, high-precision realizations cannot be achieved using solely transfer functions due to limited word length effects. The direct form structure is particularly vulnerable to quantization effects, which is a typical realization technique based on the transfer function approach. Therefore, direct form filters implemented on hardware with a limited word length are considerably degraded by quantization effects. Please see [24] and its references for further information on this subject.

Before presenting the suggested approach, the stat-space representation is described. Given an N-th order prototype filter with the transfer function $H_p(z)$, its state-space representation is as follows:

$$H_p(z) = d_p + \boldsymbol{c}_p(z\boldsymbol{I}_N - \boldsymbol{A}_P)^{-1}\boldsymbol{b}_p \tag{4.13}$$

Where $\boldsymbol{I}_N$ denotes the $N \times N$ identity matrix and $\boldsymbol{A}_p \in \Re^{N\times N}$, $\boldsymbol{b}_p \in \Re^{N\times 1}$, $\boldsymbol{c}_p \in \Re^{1\times N}$ and $d_p \in \Re$ are real-valued coefficients of the state-space filter. Using this set of coefficients, the input-output relationship for this filter is given by the following state-space equations:

$$\begin{aligned} \boldsymbol{x}(n+1) &= \boldsymbol{A}_P\boldsymbol{x}(n) + \boldsymbol{b}_p u(n) \\ y(n) &= \boldsymbol{c}_p\boldsymbol{x}(n) + d_p u(n) \end{aligned} \tag{4.14}$$

Where $u(n)$ is the input signal, $y(n)$ is the output signal and $\boldsymbol{x}(n) \in \Re^{N\times 1}$ is the state vector corresponding to the outputs of delay elements. This chapter assumes that the prototype state-space filter is asymptotically stable (i.e.. $\boldsymbol{A}_P$ Has all Eigenvalues within the unit circle), and that it is controllable and observable. This state-space filter's block diagram is seen in Figure 4.2. Here, the thick arrows indicate vector signals, while the thin arrows represent scalar signals.

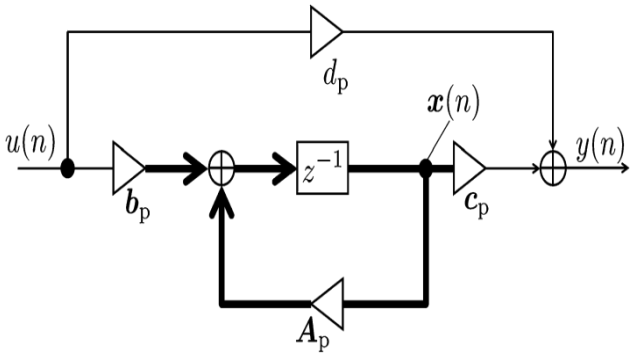

Figure 4.2 Block diagram of $H_p(z)$ in state-space form.

It is well-known that the set $(\boldsymbol{A}_P\ \boldsymbol{b}_p\ \boldsymbol{c}_p)$ is non-unique; thus, several realizations of $(\boldsymbol{A}_P\ \boldsymbol{b}_p\ \boldsymbol{c}_p)$ exist for the transfer function $H_p(z)$. Moreover, it is essential to highlight that the performance of the filter in terms of finite word length effects is dependent on the selection of the set $((\boldsymbol{A}_P\ \boldsymbol{b}_p\ \boldsymbol{c}_p))$This suggests that a suitable design of $(\boldsymbol{A}_P\ \boldsymbol{b}_p\ \boldsymbol{c}_p)$ yields a state-space filter with great performance in terms of the finite word length effects. For information, see [24] and the citations therein.

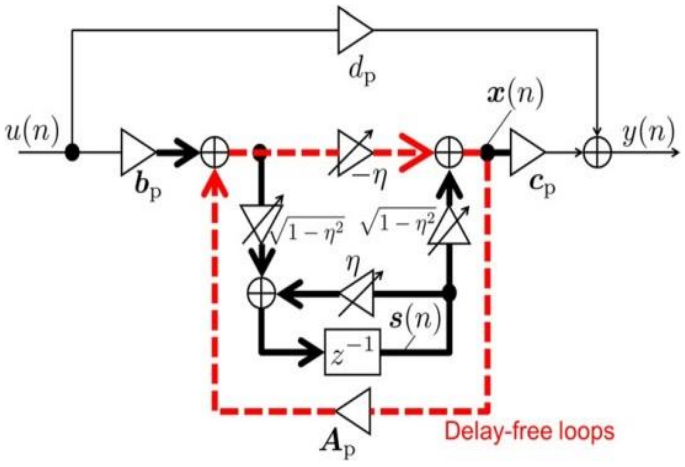

Figure 4.3 Block diagram of $H_{LP}(z,\eta)$ in state-space form with delay-free loops.

Our state-space VLPFs, VHPFs, VBPFs, and VBSFs are now shown.

4.2.1 Design of state-space Variable Low-Pass Filters (VLPFs)

The suggested technique is based on the state-space formulation of the LP-LP transformation described in [46]. Let $H_{LP}(z,\eta)$ be the transfer function of the desired VLPF as in Eq.(4.2), and let $(\boldsymbol{A}_{LP}(\eta), \boldsymbol{b}_{LP}(\eta), \boldsymbol{c}_{LP}(\eta), d_{LP}(\eta))$ be a state-space representation of $H_{LP}(z,\eta)$. Then, the set $(\boldsymbol{A}_{LP}(\eta), \boldsymbol{b}_{LP}(\eta), \boldsymbol{c}_{LP}(\eta), d_{LP}(\eta))$ can be given in terms of $(\boldsymbol{A}_P, \boldsymbol{b}_p, \boldsymbol{c}_p, d_p)$ and η as follows [46]:

$$
\begin{aligned}
\boldsymbol{A}_{LP}(\eta) &= (\eta \boldsymbol{I}_N + \boldsymbol{A}_P) + (\boldsymbol{I}_N + \eta \boldsymbol{A}_P)^{-1} \\
\boldsymbol{b}_{LP}(\eta) &= \sqrt{1-\eta^2}(\boldsymbol{I}_N + \eta \boldsymbol{A}_P)^{-1}\boldsymbol{b}_p \\
\boldsymbol{c}_{LP}(\eta) &= \sqrt{1-\eta^2}\boldsymbol{c}_p(\boldsymbol{I}_N + \eta \boldsymbol{A}_P)^{-1} \\
d_{LP}(\eta) &= d_p - \eta \boldsymbol{c}_p(\boldsymbol{I}_N + \eta \boldsymbol{A}_P)^{-1}\boldsymbol{b}_p\ .
\end{aligned}
\tag{4.15}
$$

This system is derived as described below. Figure 4.2 delay elements are first substituted with $T_{LP}(z,\eta)$, which has a normalized lattice structure [47]. The resulting structure is shown in Figure 4.3[25], where it should be noted that the normalized lattice structure realizes the all-pass filter $T_{LP}(z,\eta)$and generates delay-free loops. let $s(n) \in \Re^{N\times 1}$ represent the new state vector corresponding to Figure 4.3 delay element outputs. Then, the following relationships remain true for s$(n), u(n), y(n)$ and $\boldsymbol{x}(n)$

$$\begin{aligned} \boldsymbol{s}(n+1) &= \boldsymbol{A}_{LP}(\eta)\boldsymbol{s}(n) + \boldsymbol{b}_{LP}(\eta)u(n) \\ y(n) &= \boldsymbol{c}_{LP}(\eta)s(n) + d_{LP}(\eta)u(n) \end{aligned} \tag{4.16}$$

where $\boldsymbol{A}_{LP}(\eta), \boldsymbol{b}_{LP}, \boldsymbol{c}_{LP}(\eta)$, and d_{LP} are determined by Eq.(4.15). Although Eq.(4.15) provides a unified framework for the state-space formulation of VLPFs, this formulation is not suitable for implementation since the coefficients contain the inverse matrix $(\boldsymbol{I}_N + \eta\boldsymbol{A}_P)^{-1}$ and the square root $\sqrt{1-\eta^2}$, which significantly increases the hardware complexity. In light of this, we will revise the formulation of Eq.(4.15) using series approximations.

In this part, an efficient method based on series approximations is used in a simple algebraic formulation that minimizes the computation complexity and improves the performance of all forms of VDFs [26]. First, the needed inverse matrix is computed using a negative binomial series theory:

$$(\boldsymbol{I}_N + \eta\boldsymbol{A}_p)^{-1} = \sum_{k=0}^{\infty}\left(-\eta\boldsymbol{A}_p\right)^k. \tag{4.17}$$

Assuming that $|\eta| \ll 1$ decreases this expansion after *M* terms. It is possible to approximate the inverse matrix using the matrix $\boldsymbol{X}(\eta)$:

Where

$$\begin{aligned} \left(\boldsymbol{I}_N + \eta\boldsymbol{A}_p\right)^{-1} &= \boldsymbol{I}_N + \sum_{k=1}^{M}\left(-\eta\boldsymbol{A}_p\right)^k \\ &\simeq \boldsymbol{X}(\eta) \end{aligned} \tag{4.18}$$

Using step response with k_c Iterations, as requested by the user [50], the matrix $\boldsymbol{X}(\eta)$ is generated. When $M = k_c$, this technique corresponds to the previously suggested method and our method. Second, we use the Taylor series approximation to get a close value for the square root $\sqrt{1-\eta^2}$:

$$\sqrt{1-\eta^2} = \sum_{k=0}^{\infty} \frac{2k!(-1)^k}{(k!)^2 4^k (1-2k)} (-\eta^2)^k \tag{4.19}$$

Consequently, the square root $\sqrt{1-\eta^2}$ is approximated as $\chi(\eta)$:

$$\begin{aligned} \sqrt{1-\eta^2} &\simeq \chi(\eta) \\ &= \sum_{k=0}^{l} \frac{2k!(-1)^k}{(k!)^2 4^k (1-2k)} (-\eta^2)^k \end{aligned} \tag{4.20}$$

Where l is the user-determined parameter, and $\Phi(\xi)$ is the series approximation of $\sqrt{1-\xi^2}$, namely:

$$\Phi(\xi) = \sum_{k=0}^{R} \frac{2k!(-1)^k}{(k!)^2 4^k (1-2k)} (-\xi^2)^k. \tag{4.21}$$

The user determines the value of R.

From Eq.(4.18) and Eq.(4.20), the state-space coefficients of VLPFs can be given in terms of $(\boldsymbol{A}_p, \boldsymbol{b}_p, \boldsymbol{c}_p, d_p)$ and η as follows:

$$\begin{aligned} \boldsymbol{A}_{LP}(\eta) &= \left(\eta \boldsymbol{I}_N + \boldsymbol{A}_p\right) \boldsymbol{X}(\eta) \\ \boldsymbol{b}_{LP}(\eta) &= \chi(\eta) \boldsymbol{X}(\eta) \boldsymbol{b}_p \\ \boldsymbol{c}_{LP}(\eta) &= \chi(\eta) \boldsymbol{c}_p \, \boldsymbol{X}(\eta) \\ d_{LP}(\eta) &= d_p - \eta \boldsymbol{c}_p \boldsymbol{X}(\eta) \boldsymbol{b}_p. \end{aligned} \tag{4.22}$$

4.2.2 Design of state-space Variable High-Pass Filters (VHPFs)

Applying the LP-HP transformation [3] transforms a prototype low-pass filter $H_p(z)$ into a high-pass filter $H_{HP}(z, \eta)$ with an all-pass function $T_{HP}(z, \eta)$ to get the desired

transfer function $H_{HP}(z,\eta)$:

$$H_{HP}(z,\eta) = H_p(z)|_{z^{-1}\leftarrow T_{HP}(z,\eta)}$$
$$T_{HP}(z,\eta) = -\frac{z^{-1}+\eta}{1+\eta z^{-1}} \tag{4.23}$$

The parameter η adjusts the bandwidth of the transfer function $H_{HP}(z,\eta)$ in the same way, as described in the preceding subsection. The following definition applies to the coefficients of variable high-pass filters (VHPFs):

$$\begin{aligned}\boldsymbol{A}_{HP}(\eta) &= -\left(\eta \boldsymbol{I}_N + \boldsymbol{A}_p\right)\boldsymbol{X}(\eta)\\ \boldsymbol{b}_{HP}(\eta) &= \chi(\eta)\boldsymbol{X}(\eta)\boldsymbol{b}_p\\ \boldsymbol{c}_{HP}(\eta) &= -\chi(\eta)\boldsymbol{c}_p\boldsymbol{X}(\eta)\\ d_{HP}(\eta) &= d_p - \eta\boldsymbol{c}_p\boldsymbol{X}(\eta)\boldsymbol{b}_p\end{aligned} \tag{4.24}$$

4.2.3 Design of state-space Variable Band-Pass Filters (VBPFs)

$H_{BP}(z,\eta,\xi)$ represents the transfer function of the needed VBPFs. Consequently, VBPFs are built with a two-step frequency transformation, the first is based on LP-LP transformation, and the second is based on LP-BP transformation [22]:

$$\begin{aligned}H_{BP}(z,\eta,\xi) &= \widetilde{H}_P(z,\eta)|_{z^{-1}\leftarrow T_{BP2}(z,\xi)}\\ \widetilde{H}_P(z,\eta) &= H_P(z)|_{z^{-1}\leftarrow T_{BP1}(z,\eta)}\\ T_{BP1}(z,\eta) &= T_{LP}(z,\eta)\\ T_{BP2}(z,\xi) &= -z^{-1}\frac{z^{-1}-\xi}{1-\xi z^{-1}},\ |\xi|<1\end{aligned} \tag{4.25}$$

Step1: The state-space VLPFs $(\boldsymbol{A}_{LP}(\eta), \boldsymbol{b}_{LP}(\eta), \boldsymbol{c}_{LP}(\eta), d_{LP}(\eta))$ is established from the prototype state-space $(\boldsymbol{A}_p, \boldsymbol{b}_p, \boldsymbol{c}_p, d_p)$ using Eq.(4.22).

Step2: Replace $(\boldsymbol{A}_p, \boldsymbol{b}_p, \boldsymbol{c}_p, d_p)$ with the set $(\boldsymbol{A}_{LP}(\eta), \boldsymbol{b}_{LP}(\eta), \boldsymbol{c}_{LP}(\eta), d_{LP}(\eta))$ mentioned above in Eq(20) of [24], and applying the series approximation to the terms $\sqrt{1-\xi^2}$. As a consequence, the new state space VBPFs is as follows:

$$\begin{aligned}
\boldsymbol{A}_{BP}(\eta,\xi) &= \begin{pmatrix} \xi \boldsymbol{I}_N & -\Phi(\xi)\big(\eta \boldsymbol{I}_N + \boldsymbol{A}_p\big)\boldsymbol{X}(\eta) \\ \Phi(\xi)\boldsymbol{I}_N & \xi(\eta \boldsymbol{I}_N + \boldsymbol{A}_p)\boldsymbol{X}(\eta) \end{pmatrix} \\
\boldsymbol{b}_{BP}(\eta,\xi) &= \begin{pmatrix} \Phi(\xi)\chi(\eta)\boldsymbol{X}(\eta)\boldsymbol{b}_p \\ -\xi\chi(\eta)\boldsymbol{X}(\eta)\boldsymbol{b}_p \end{pmatrix} \\
\boldsymbol{c}_{BP}(\eta,\xi) &= \begin{pmatrix} \boldsymbol{0}_{1\times N} & -\chi(\eta)\boldsymbol{c}_p\boldsymbol{X}(\eta) \end{pmatrix} \\
d_{BP}(\eta) &= d_p - \eta \boldsymbol{c}_p \boldsymbol{X}(\eta)\boldsymbol{b}_p
\end{aligned} \tag{4.26}$$

where $\boldsymbol{0}_{1\times N}$ denotes the $1 \times N$ zero matrix, and ξ and η are the parameters for tunning the center frequency and pass-band bandwidth, respectively. For $\eta > 0$, the pass bandwidth drops, but it increase for $\eta < 0$. For $\xi < 0$, the central frequency rises, but it drops for $\xi > 0$. The state-space VBPFs stated in Eq. (4.26) tune both the center frequency and bandwidth, as opposed to the state-space VBPFs specified in [24], which only tune the center frequency.

4.2.4 Design of state-space Variable Band-Stop Filters (VBSFs)

$H_{BS}(z,\eta,\xi)$ should serve as the transfer function for VBSFs. Using two-phase transformations, the transfer function of $H_{BS}(z,\eta,\xi)$ is obtained as follows:

$$\begin{aligned}
H_{BS}(z,\eta,\xi) &= \widetilde{H}_P(z,\eta)|_{z^{-1}\leftarrow T_{BS2}(z,\xi)} \\
\widetilde{H}_P(z,\eta) &= H_P(z)|_{z^{-1}\leftarrow T_{BS1}(z,\eta)} \\
T_{BS1}(z,\eta) &= T_{LP}(z,\eta) \\
T_{BS2}(z,\xi) &= z^{-1}\frac{z^{-1} - \xi}{1 - \xi z^{-1}} \quad |\xi| < 1
\end{aligned} \tag{4.27}$$

If $\eta > 0$, the output stop bandwidth is larger than the output of the prototype filter, and if $\eta < 0$, it is smaller. Similar to how it works with VBPFs, the parameter ξ adjusts the center frequency. Consequently, the following are the state-space coefficients of VBSFs:

$$\boldsymbol{A}_{BS}(\eta,\xi)=\begin{pmatrix}\xi\boldsymbol{I}_N & \Phi(\xi)\big(\eta\boldsymbol{I}_N+\boldsymbol{A}_p\big)\boldsymbol{X}(\eta)\\ \Phi(\xi)\boldsymbol{I}_N & -\xi(\eta\boldsymbol{I}_N+\boldsymbol{A}_p)\boldsymbol{X}(\eta)\end{pmatrix}$$
$$\boldsymbol{b}_{BS}(n,\xi)=\begin{pmatrix}\Phi(\xi)\chi(\eta)\boldsymbol{X}(\eta)\boldsymbol{b}_p\\ -\xi\chi(\eta)\boldsymbol{X}(\eta)\boldsymbol{b}_p\end{pmatrix}$$
$$\boldsymbol{c}_{BS}(\eta,\xi)=\begin{pmatrix}-\boldsymbol{0}_{1\times N} & \chi(\eta)\boldsymbol{c}_p\boldsymbol{X}(\eta)\end{pmatrix} \tag{4.28}$$
$$d_{BS}(\eta)=d_p-\eta\boldsymbol{c}_p\boldsymbol{X}(\eta)\boldsymbol{b}_p\ .$$

4.3 Conclusion

This chapter proposes and describes a straightforward, efficient state-space-based technique for designing and realizing variable IIR digital filters with high-precision tuning. State-space-based frequency transformation was used to produce the variable filters. Calculating the inverse matrix and square root was necessary for this transformation to construct a basic state-space VDF without any computational complexity.

Chapter 5

Results and discussions

5.1 Introduction

This chapter describes the utility of the suggested technique and compares it to the earlier methods [24, 25]. Then, each VLPF output is evaluated based on the approximation error. In addition, we examine the frequency response performances of various types of digital filters, including VLPFs, VHPFs, VBPFs, and VBSFs.

5.2 Numerical examples

5.2.1 Approximation error

We evaluate each VLPFs performance based on its approximation error. First, the definition of the approximation error is as follows:

$$PE = max_{\omega}\left|H_{LP}\left(e^{j\omega},\eta\right) - \widehat{H}_{LP}(e^{j\omega},\eta)\right| \quad (5.1)$$

$\widehat{H}_{LP}\left(e^{j\omega},\eta\right)$ is the approximated transfer function for the VLPFs for the proposed technique, while $H_{LP}\left(e^{j\omega},\eta\right)$ is the ideal transfer function for the VLPFs (not approximated). The used low-pass prototype filter is a fifth-order low-pass elliptic filter with the transfer function shown below:

$$H_p(z) = \frac{0.0222-0.0128z^{-1}+0.0212z^{-2}+0.0212z^{-3}-0.0128z^{-4}+0.0222z^{-5}}{1-3.3424z^{-1}+5.1483z^{-2}-4.3513z^{-3}+2.0111z^{-4}-0.4045z^{-5}}. \quad (5.2)$$

The pass-band ripple, stop-band ripple, and pass-band edge frequency elliptic digital filters are respectively set to 0.5 dB, 40 dB, and 0.25π. These are the state-space coefficients of this prototype filter:

$$\boldsymbol{A}_p = \begin{pmatrix} 0.8504 & 0.4403 & -0.0231 & -0.0689 & 0.0060 \\ -0.4403 & 0.6904 & -0.4246 & 0.0330 & -0.0553 \\ -0.0231 & 0.4246 & 0.6177 & 0.4105 & -0.0482 \\ 0.0689 & 0.0330 & -0.4105 & 0.5709 & 0.3969 \\ 0.0060 & 0.0553 & -0.0482 & -0.3969 & 0.6130 \end{pmatrix}$$

$$\boldsymbol{b}_p = (0.3346\ 0.3547 - 0.3198 - 0.1841 - 0.0838)^T$$

$$\boldsymbol{c}_p = (0.3346 - 0.3547 - 0.3198\ 0.1841 - 0.0838) \qquad (5.3)$$

$$d_p = 0.0222\ .$$

In order to realize the low-pass digital filters, the values M = 1 or $M = 3$ and $l = 8$ have been selected. Figure 5.1 illustrates the assessment outcomes for $-0.2 \leq \eta \leq 0.2$. When $M = 3$, the suggested technique gives an approximation error much smaller than the prior method when $M = 1$and $M = 3$. Thus, the proposed algorithm provides a good approximation by developing the approximation of state-space coefficients.

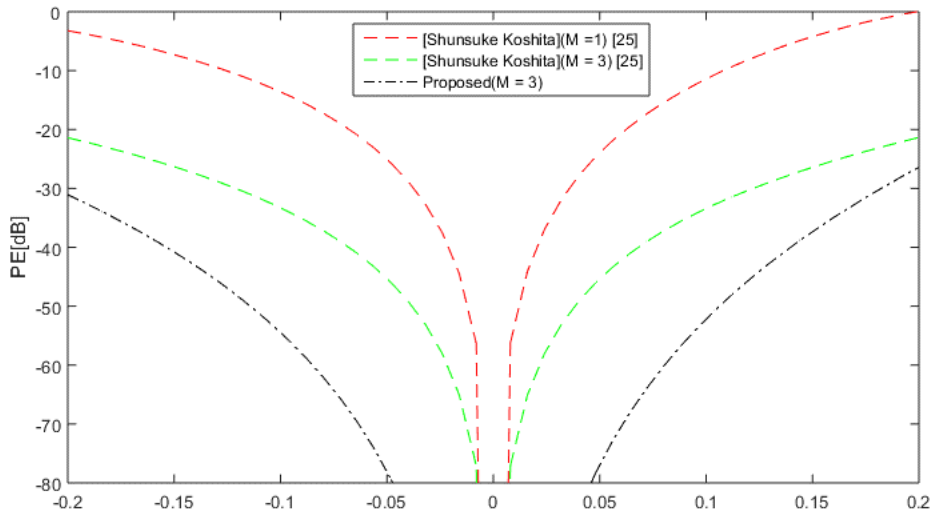

Figure 5.1 Evaluation of approximation errors of VLPFs: Peak errors.

5.2.2 Evaluation of performance for high-order narrow band VDFS

High-order narrow-band IIR filters, which are challenging to design and serve crucial roles in various applications, are very prone to quantization effects, resulting in significant

frequency response deterioration. Thus, a narrow, high-order band would illustrate the suggested method's practical utility. The response error is defined as follows:

$$\text{Absolute error} = \left|H(e^{j\omega},\eta) - \widehat{H}(e^{j\widehat{\omega}},\eta)\right| \tag{5.4}$$

$H_{LP}(e^{j\omega},\eta)$ is the frequency response indicated by the proposed technique and the prior approach, given that $\widehat{H}_{LP}(e^{j\omega},\eta)$ is the ideal response at frequency without approximations and coefficient quantization. Eight fractional bits are quantized into the filter coefficients. All VDFs (VLPFs, VHPFs, VBPFs, and VBSFs) are used in this part. The prototype low-pass filter is a 10th-order elliptic filter with 1 dB peak-to-peak ripple, 40 dB minimum stop-band attenuation, and 0.15 rad pass-band edge frequency.

5.2.2.1 Example 1

In this example, we provide a comparison between proposed method [26] and the conventional method that depends on the structure of a cascaded direct form, also with the previous method published in [25], the filters used here are the VLPFs and the VHPFs.

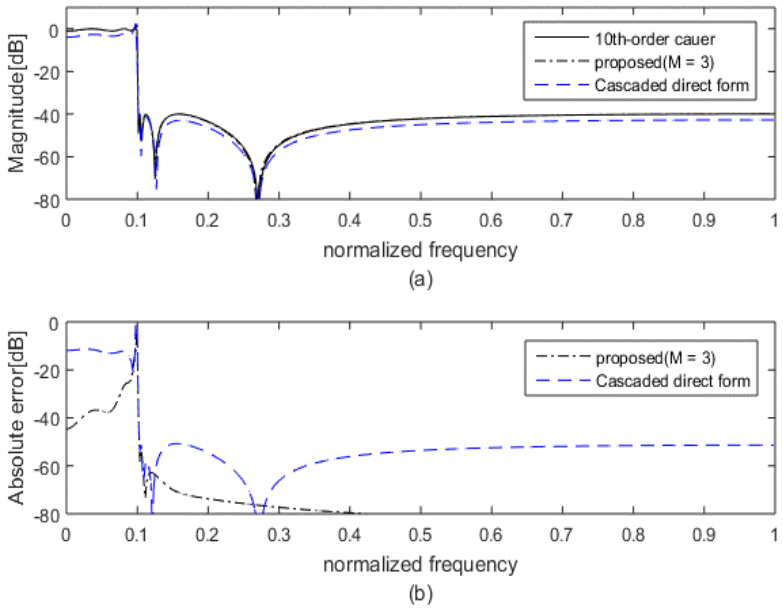

Figure 5.2 Evaluation results for 10th-order narrow-band VLPFs: (a) Magnitude responses and (b) Error responses for $\eta = 0.2, l = 8$.

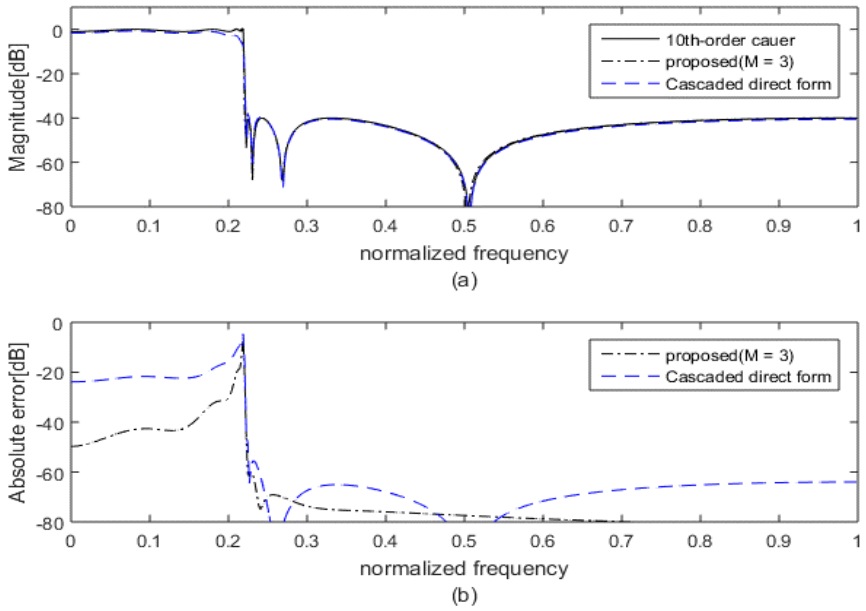

Figure 5.3 Evaluation results for 10th-order narrow-band VLPFs: (a) Magnitude responses and (b) Error responses for $\eta = -0.2, l = 12$.

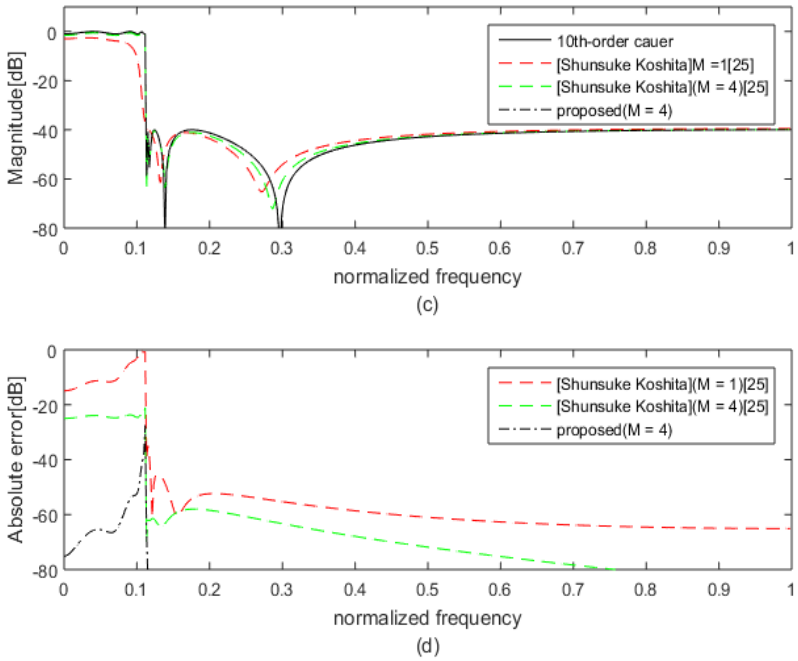

Figure 5.4 Evaluation results for 10th-order narrow-band VLPFs: (c) Magnitude responses and (d) Error responses for $\eta = 0.15, l = 12$.

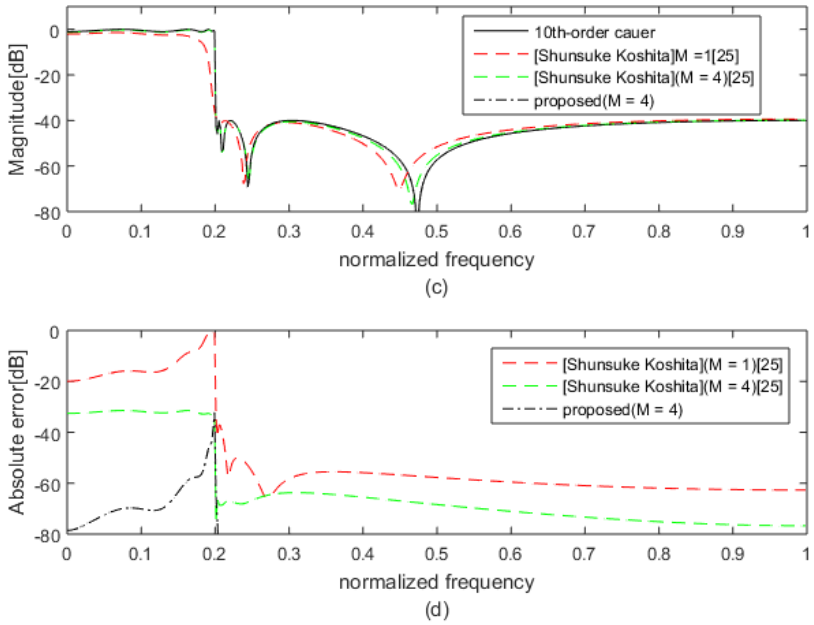

Figure 5.5 Evaluation results for 10th-order narrow-band VLPFs: (c) Magnitude responses and (d) Error responses for $\eta = -0.15, l = 4$.

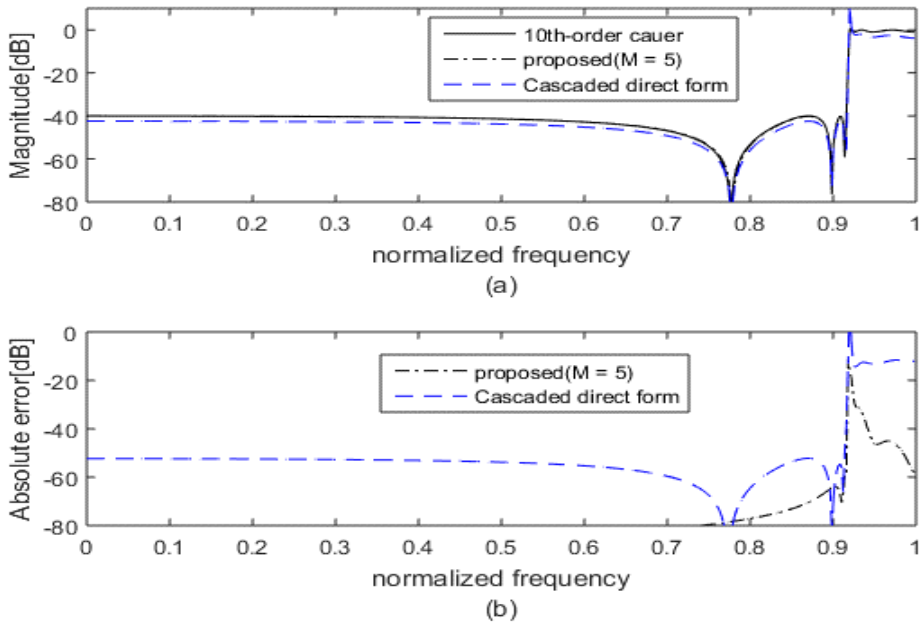

Figure 5.6 Evaluation results for 10th-order narrow-band VHPFs: (a) Magnitude responses and (b) Error responses for $\eta = 0.3, l = 8$.

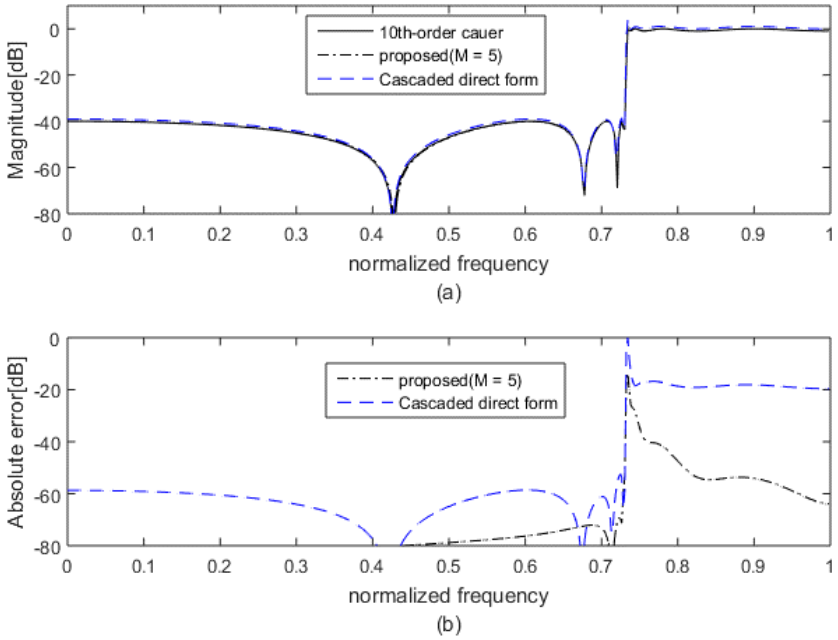

Figure 5.7 Evaluation results for 10th-order narrow-band VHPFs: (a) Magnitude responses and (b) Error responses for $\eta = -0.3, l = 12$.

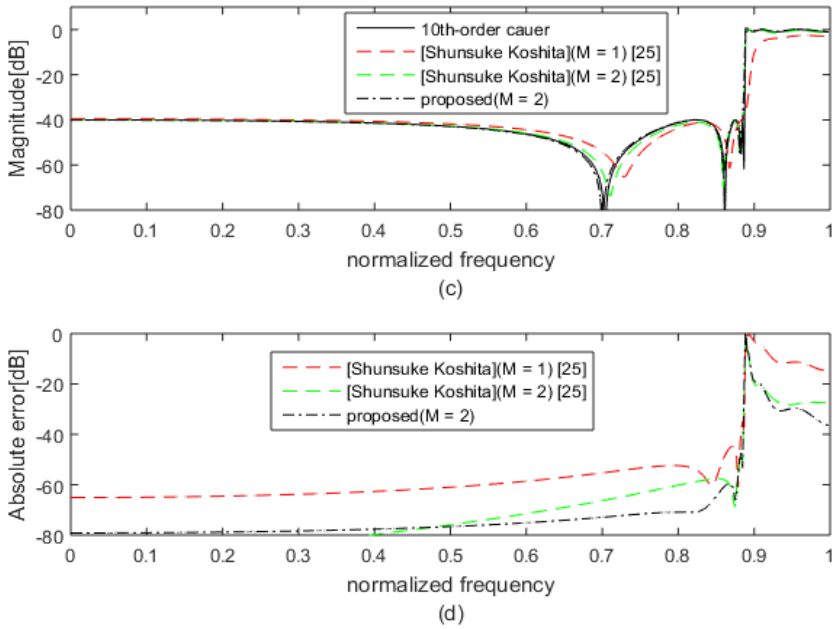

Figure 5.8 Evaluation results for 10th-order narrow-band VHPFs: (c) Magnitude responses and (d) Error responses for $\eta = 0.15, l = 12$.

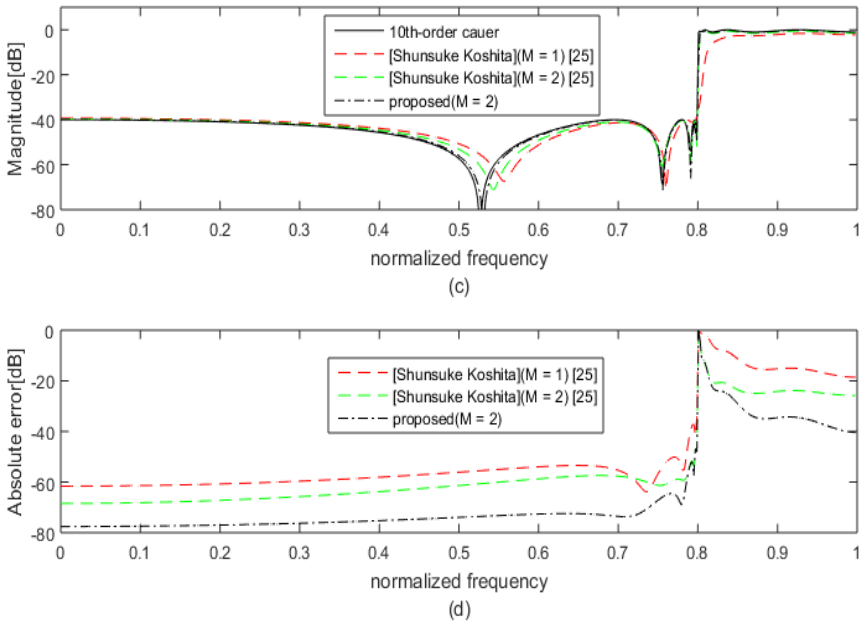

Figure 5.9 Evaluation results for 10th-order narrow-band VHPFs: (c) Magnitude responses and (d) Error responses for $\eta = -0.15, l = 8$.

Figures 5.2–5.9 illustrate the evaluation results for the VLPFs and the VHPFs, respectively. In addition, the frequency responses to the proposed methods show good agreement with the ideal responses, for the VLPFs and the VHPFs. The previous approach [25] has lower accuracy than the proposed method for $M = 2$ and $M = 4$, as shown in Figures 5.4 and 5.5 for VLPFs, and Figures 5.8 and 5.9 for VHPFS. Furthermore, the magnitude responses of cascaded direct form are less than our technique, as shown in Figures 5.2 and 5.3 for VLPFs, and Figures 5.6 and 5.7 for VHPFS. As well-known, the direct form realization is very sensitive to quantization effects.

5.2.2.2 Example 2

In this example, we compare our proposed method to the previous method based on Gramian-preserving frequency transformation [24] and the previous method published in [25], where the filters used are the VBPFs and VBSFs.

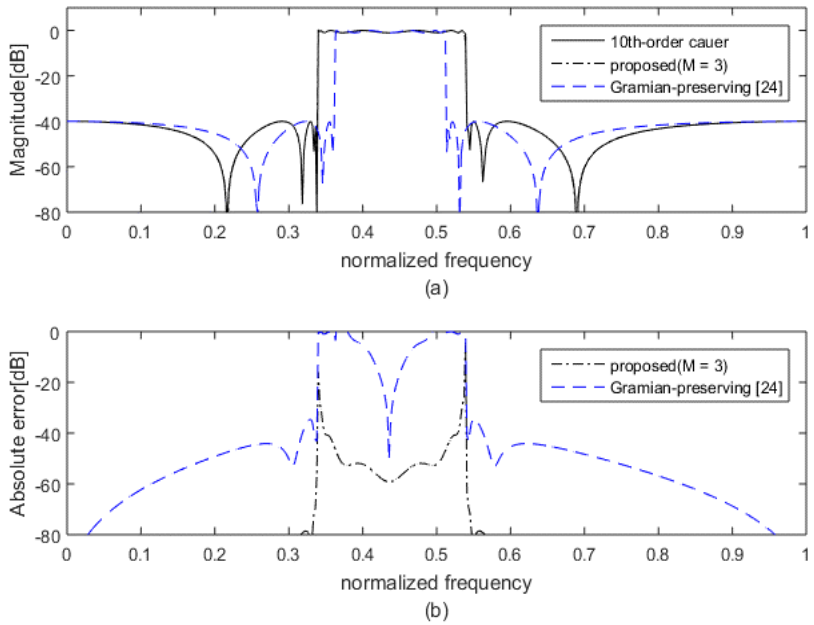

Figure 5.10 Evaluation results for 10th-order narrow-band VBPFs: (a) Magnitude responses and (b) Error responses for $\eta = -0.15, \xi = 0.20, l = 8$, and $R = 8$.

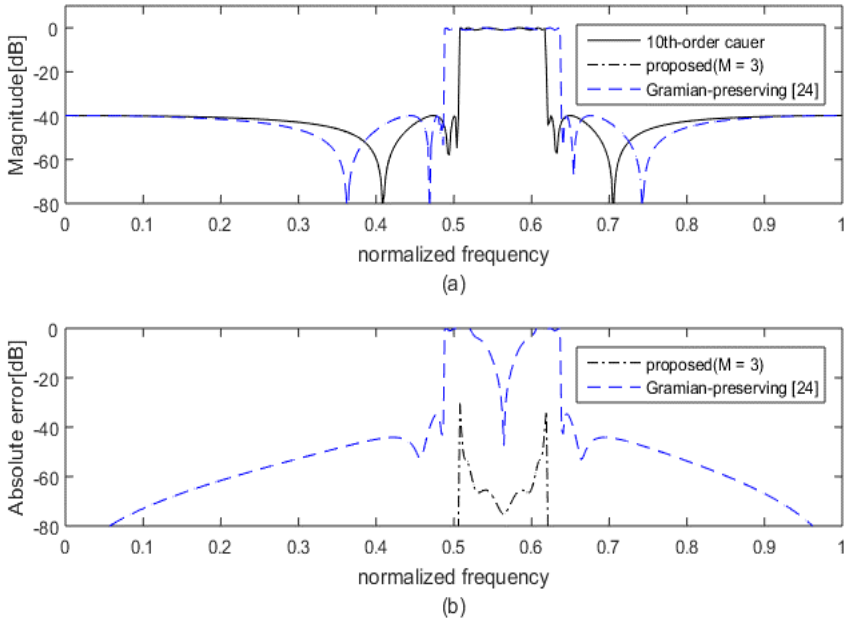

Figure 5.11 Evaluation results for 10th-order narrow-band VBPFs: (a) Magnitude responses and (b) Error responses for $\eta = 0.15, \xi = -0.20, l = 8$, and $R = 8$.

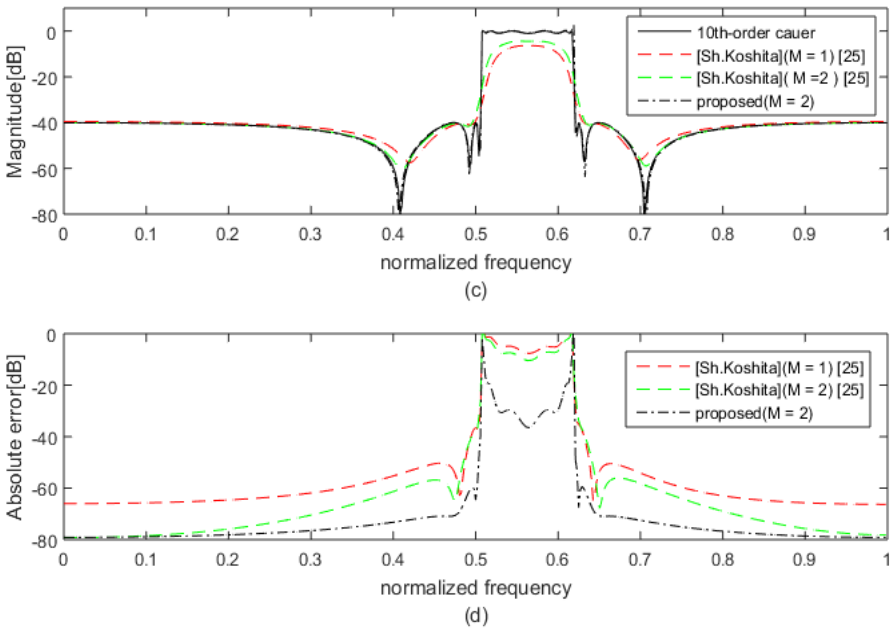

Figure 5.12 Evaluation results for 10th-order narrow-band VBPFs: (c) Magnitude responses and (d) Error responses for $\eta = 0.15, \xi = -0.20, l = 4$, and $R = 4$.

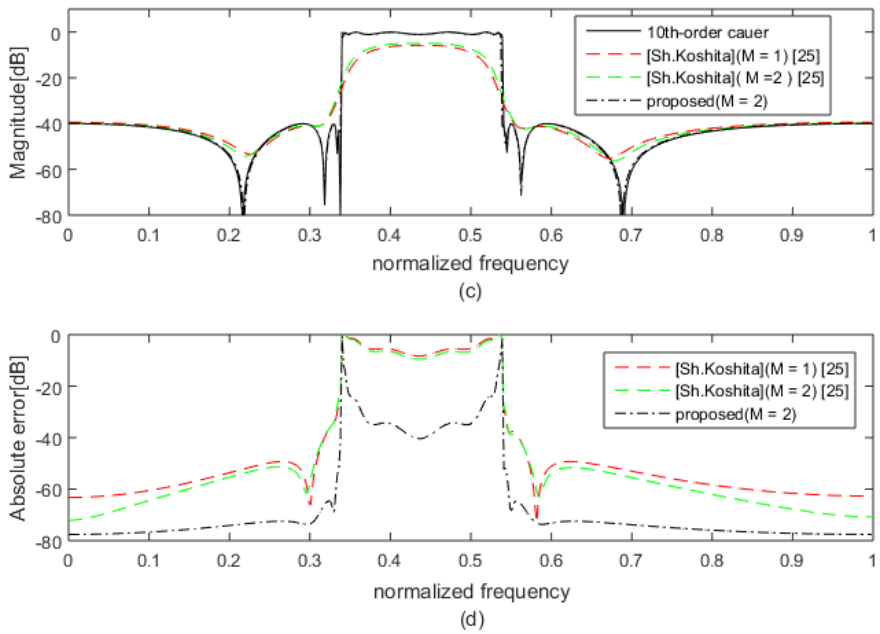

Figure 5.13 Evaluation results for 10th-order narrow-band VBPFs: (c) Magnitude responses and (d) Error responses for $\eta = -0.15, \xi = 0.20, l = 8$, and $R = 8$.

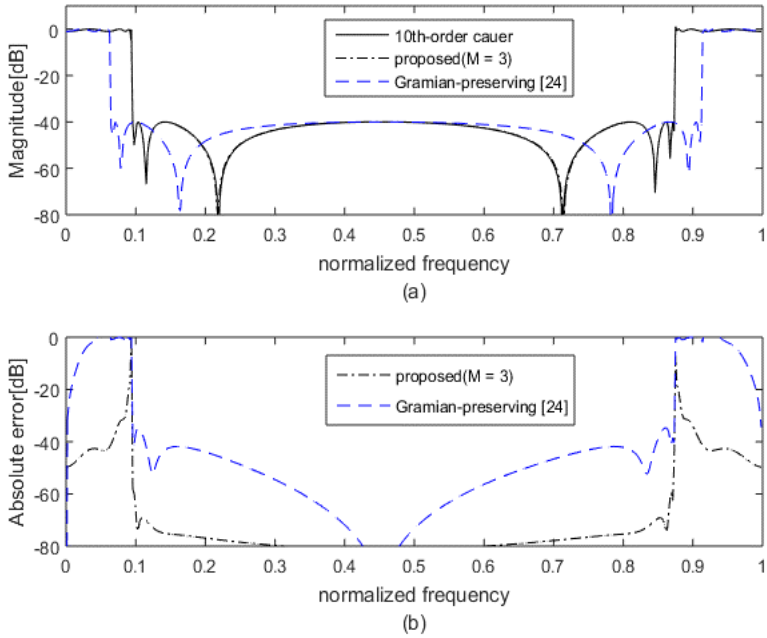

Figure 5.14 Evaluation results for 10th-order narrow-band VBSFs: (a) Magnitude responses and (b) Error responses for $\eta = -0.20, \xi = 0.15, l = 8$, and $R = 8$.

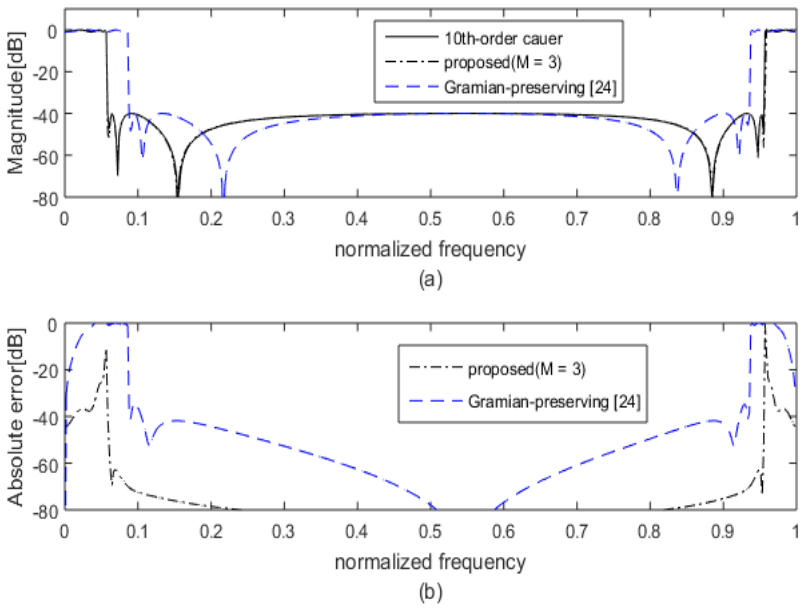

Figure 5.15 Evaluation results for 10th-order narrow-band VBSFs: (a) Magnitude responses and (b) Error responses for $\eta = 0.20, \xi = -0.15, l = 4$, and $R = 4$.

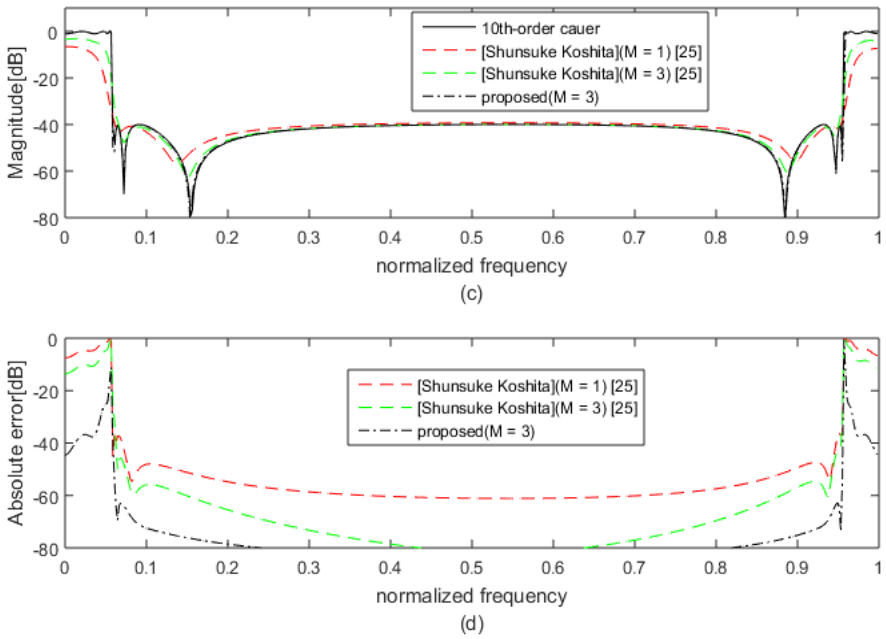

Figure 5.16 Evaluation results for 10th-order narrow-band VBSFs: (c) Magnitude responses and (d) Error responses for $\eta = 0.20, \xi = -0.15, l = 4$, and $R = 4$.

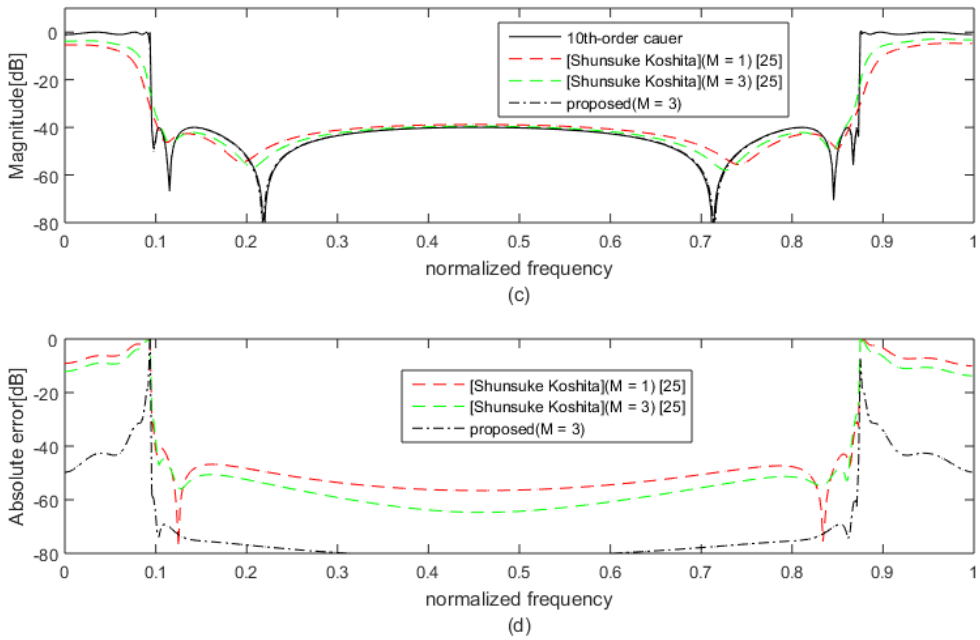

Figure 5.17 Evaluation results for 10th-order narrow-band VBSFs: (c) Magnitude responses and (d) Error responses for $\eta = -0.20, \xi = 0.15, l = 8$, and $R = 8$.

Figures 5.10-5.17 depict the corresponding assessment findings for VBPFs and VBSFs. Also shown are the frequency responses of the suggested approaches and the ideal frequency responses. For all VDFs, The results in the proposed method are highly in agreement with the ideal method, In addition, the previous technique [25] is less precise than the one provided for M = 2 and $M = 3$ as shown in Figures 5.12 and 5.13 for VBPFs, Figures 5.16 and 5.17 for VBSFs. In addition, Figures 5.10 and 5.11 for VBPFs, and Figures 5.14 and 5.15 for VBSFs illustrate that the approach based on Gramian-preserving frequency transformation [24] adjusts only the central frequency with fixed bandwidth.

Despite the fact that the large value of the approximation parameter l has no effect on the computational complexity of $\chi(\eta)$ in [25], it remains a serious concern since performance deterioration is associated with reduced accuracy in approximating $\chi(\eta)$, as shown for the VBPFs and VBSFs. This recognized disadvantage is a result of the Maclaurin series, but it may be addressed by using the Taylor approximation series to get the square root. As shown in these cases, the approximation parameter l is not specified and yields a high-precision approximation of $\chi(\eta)$. These results demonstrate the efficacy of our suggested tuning precision method for limited word lengths, including high-order and narrow-band VDFs.

5.3 Conclusion

In this chapter, we presented many examples to compare the previous methods and our proposed method. The results showed that our method is better than other methods. A series approximation incorporating the negative binomial and Taylor series approximations was used. The parameters M and l may be used to modify the accuracy of the inverse matrix and square root approximations. Therefore, this method delivers great tuning accuracy regarding the finite word length for all types of VDFs.

General conclusion

A fundamental aspect of signal processing is filtering. With the aid of computer programs performing filter design algorithms, designing filters can be done relatively quickly. This modest research was based on the design of IIR digital filters using series approximations.

This work has reviewed recent research activities on VDFs, focusing on the approximation problem, the realization problem, and the applications of adaptive filtering. The results given in this thesis are based on the state-space representation, which has revealed many useful properties with respect to the performance of filters dominated by the internal properties and the input-output relationship. In particular, the Gramian-preserving frequency transformation is very attractive for designing and synthesizing high-performance filters. Using this new frequency transformation, we have presented variable digital filters that retain high performance regardless of the frequency characteristics change. The proposed method is based on the binomial series approximation and the Taylor series approximation to the state-space formulation of frequency transformations. This approach has enabled the state-space VDFs to be simultaneously realized without needing the inverse matrix and the square root.

The conventional state-space VDFs require restrictions on the transfer functions, state-space representations and tuning characteristics, whereas the proposed method is free from such restrictions. In addition, in the proposed method, the approximation accuracy can be easily controlled by the parameters M and l, leading to high-performance VDFs concerning both the approximation error and the finite wordlength effects. As discussed in the last chapter.

A low-pass, high-pass, band-pass, and band-stop IIR digital filter design examples are considered to investigate the filter's performance with the new method and compare the proposed methods' performance. A comparison was made with VDFs based on Gramian frequency transformation, cascade direct form structure, and other proposed methods. The

approximation results are better than those of other recent methods. Furthermore, this approach achieves good performance with high tuning accuracy concerning the finite wordlength effect for all types of VDFs.

Finally, since many results based on the state-space representation are reported for two-dimensional frequency transformations [31], applying these results to VDF theory may yield high-performance two-dimensional state-space VDFs. Furthermore, the proposed VDFs may be applied to the adaptive band-pass/band-stop filtering [21], leading to the new adaptive band-pass/band-stop filters that significantly improve the performance with respect to the finite wordlength effects.

Bibliography

[1] Meyer-Baese, U., & Meyer-Baese, U. (2007). *Digital signal processing with field programmable gate arrays* (Vol. 65). Berlin: springer.

[2] Stoyanov, G., & Kawamata, M. (1997). Variable digital filters. J. Signal Processing, 1(4), 275-289.

[3] Constantinides, A. G. (1970, August). Spectral transformations for digital filters. In *Proceedings of the Institution of Electrical Engineers* (Vol. 117, No. 8, pp. 1585-1590). IET Digital Library.

[4] Koshita, S., Abe, M., & Kawamata, M. (2013). Frequency transformation for linear state-space systems and its application to high-performance analog/digital filters,". InTech.

[5] Yan, S., Sun, L., Xu, L., Cai, Y., & Zhao, Q. (2018). State-space formulation of 2-D frequency transformation in Fornasini–Marchesini second model. *Multidimensional Systems and Signal Processing*, *29*(1), 361-383.

[6] Zarour, R., & Fahmy, M. M. (1989). A design technique for variable digital filters. *IEEE Transactions on circuits and systems*, *36*(11), 1473-1478.

[7] Deng, T. B. (1997). Design of recursive 1-D variable filters with guaranteed stability. *IEEE Transactions on Circuits and Systems II: Analog and Digital Signal Processing*, *44*(9), 689-695.

[8] Pun, C. K., Chan, S. C., Yeung, K. S., & Ho, K. L. (2002). On the design and implementation of FIR and IIR digital filters with variable frequency characteristics. *IEEE Transactions on Circuits and Systems II: Analog and Digital Signal Processing*, *49*(11), 689-703.

[9] Deng, T. B. (2004). Closed-form design and efficient implementation of variable digital filters with simultaneously tunable magnitude and fractional delay. *IEEE Transactions on Signal Processing*, *52*(6), 1668-1681.

[10] Koshita, S., Abe, M., & Kawamata, M. (2018, May). Minimum roundoff noise realization for variable IIR digital filters based on MD polynomial approximation. In *2018 IEEE International Symposium on Circuits and Systems (ISCAS)* (pp. 1-5). IEEE.

[11] Darak, S. J., Prasad, V. A., & Lai, E. M. K. (2012). Efficient implementation of reconfigurable warped digital filters with variable low-pass, high-pass, bandpass, and bandstop responses. *IEEE Transactions on very large scale integration (VLSI) systems*, *21*(6), 1165-1169.

[12] Darak, S. J., Vinod, A. P., Lai, E. K., Palicot, J., & Zhang, H. (2014). Linear-phase VDF design with unabridged bandwidth control over the Nyquist band. *IEEE Transactions on Circuits and Systems II: Express Briefs*, *61*(6), 428-432.

[13] Darak, S. J., Gopi, S. K. P., Prasad, V. A., & Lai, E. (2013). Low-complexity reconfigurable fast filter bank for multi-standard wireless receivers. *IEEE Transactions on Very Large Scale Integration (VLSI) Systems*, *22*(5), 1202-1206.

[14] Darak, S. J., Palicot, J., Zhang, H., Prasad, V. A., & Moy, C. (2014). Reconfigurable filter bank with complete control over subband bandwidths for multistandard wireless communication receivers. *IEEE Transactions on Very Large Scale Integration (VLSI) Systems*, *23*(9), 1772-1782.

[15] Darak, S. J., Dhabu, S., Moy, C., Zhang, H., Palicot, J., & Vinod, A. P. (2015). Low complexity and efficient dynamic spectrum learning and tunable bandwidth access for heterogeneous decentralized cognitive radio networks. *Digital Signal Processing*, *37*, 13-23.

[16] Yu, Y. J., Lim, Y. C., & Shi, D. (2008). Low-complexity design of variable bandedge linear phase FIR filters with sharp transition band. *IEEE Transactions on Signal Processing*, *57*(4), 1328-1338.

[17] Yu, Y. J., & Xu, W. J. (2011). Mixed-radix fast filter bank approach for the design of variable digital filters with simultaneously tunable bandedge and fractional delay. *IEEE transactions on signal processing*, *60*(1), 100-111.

[18] Xu, W. J., Yu, Y. J., & Johansson, H. (2014). Improved filter bank approach for the design of variable bandedge and fractional delay filters. *IEEE Transactions on Circuits and Systems I: Regular Papers*, *61*(3), 764-777.

[19] Chambers, J. A., & Constantinides, A. G. (1990, December). Frequency tracking using constrained adaptive notch filters synthesised from allpass sections. In *IEE Proceedings F (Radar and Signal Processing)* (Vol. 137, No. 6, pp. 475-481). IET Digital Library.

[20] DeBrunner, V., & Torres, S. (2000). Multiple fully adaptive notch filter design based on allpass sections. *IEEE transactions on Signal Processing*, *48*(2), 550-552.

[21] Koshita, S., Kumamoto, Y., Abe, M., & Kawamata, M. (2013). Adaptive IIR band-pass/band-stop filtering using high-order transfer function and frequency transformation. *Interdisciplinary Information Sciences*, *19*(2), 163-172.

[22] El-Ghoroury, H., & Gupta, S. (1976). Wave digital filter structures with variable frequency characteristics. *IEEE Transactions on Circuits and Systems*, *23*(10), 624-630.

[23] Matsukawa, H., & Kawamata, M. (2001). Design of variable digital filters based on state-space realizations. *IEICE Transactions on Fundamentals of Electronics, Communications and Computer Sciences*, *84*(8), 1822-1830.
[24] Koshita, S., Miyoshi, K., Abe, M., & Kawamata, M. (2014). High-performance variable band-pass/band-stop state-space digital filters using Gramian-preserving frequency transformation. *Digital Signal Processing*, *27*, 175-184.
[25] Koshita, S., Abe, M., & Kawamata, M. (2017). Variable state-space digital filters using series approximations. *Digital Signal Processing*, *60*, 338-349.
[26] Rahmani, I., Mitiche, L., & Adamou-Mitiche, A. B. H. (2022). Improved state-space all-digital filters via series approximations. *Journal of Circuits, Systems and Computers*,31(13),225-238.
[27] Hersent, O., Gurle, D., & Petit, J. P. (2000). *IP Telephony: Packet-based multimedia communications systems*. Addison-Wesley Professional.
[28] http://people.rennes.inria.fr/Olivier.Sentieys/teach/MainPoly_TDDS.pdf
[29] Roberts, R. A., & Mullis, C. T. (1987). *Digital signal processing*. Addison-Wesley Longman Publishing Co., Inc..
[30] Mitra, S. K., Neuvo, Y., & Roivainen, H. (1990). Design of recursive digital filters with variable characteristics. *International journal of circuit theory and applications*, *18*(2), 107-119.
[31] Jang, H. J., & Kawamata, M. (2002). Realization of high accuracy 2-D variable IIR digital filters. *IEICE Transactions on Fundamentals of Electronics, Communications and Computer Sciences*, *85*(10), 2293-2301.
[32] Watanabe, E., Ito, M., Murakoshi, N., & Nishihara, A. (1994). A synthesis of variable wave digital filters. *IEICE Transactions on Fundamentals of Electronics, Communications and Computer Sciences*, *77*(1), 263-271.
[33] Farrow, C. W. (1988, June). A continuously variable digital delay element. In *1988., IEEE International Symposium on Circuits and Systems* (pp. 2641-2645). IEEE.
[34] Stoyanov, G., Uzunov, I., & Kawamata, M. (2001). Design and realization of variable IIR digital filters as a cascade of identical subfilters. *IEICE Transactions on Fundamentals of Electronics, Communications and Computer Sciences*, *84*(8), 1831-1839.
[35] Regalia, P. A., Mitra, S. K., & Vaidyanathan, P. P. (1988). The digital all-pass filter: A versatile signal processing building block. *Proceedings of the IEEE*, *76*(1), 19-37.
[36] Regalia, P. (1994). *Adaptive IIR Filtering in Signal Processing and Control* (Vol. 90). CRC Press.
[37] Regalia, P. A. (2010). A complex adaptive notch filter. *IEEE Signal Processing Letters*, *17*(11), 937-940.
[38] Chen, W. K. (1995). The circuits and filters handbook.
[39] Snelgrove, W., & Sedra, A. (1986). Synthesis and analysis of state-space active filters using intermediate transfer functions. *IEEE transactions on circuits and systems*, *33*(3), 287-301.
[40] Mullis, C., & Roberts, R. (1976). Synthesis of minimum roundoff noise fixed point digital filters. *IEEE Transactions on Circuits and Systems*, *23*(9), 551-562.
[41] Yamaki, S., Abe, M., & Kawamata, M. (2008). A closed form solution to L 2-sensitivity minimization of second-order state-space digital filters. *IEICE transactions on fundamentals of electronics, communications and computer sciences*, *91*(5), 1268-1273.
[42] Hwang, S. (1977). Minimum uncorrelated unit noise in state-space digital filtering. *IEEE Transactions on Acoustics, Speech, and Signal Processing*, *25*(4), 273-281.
[43] Tavsanoglu, V., & Thiele, L. (1984). Optimal design of state-space digital filters by simultaneous minimization of sensitivity and roundoff noise. *IEEE transactions on circuits and systems*, *31*(10), 884-888.
[44] Pernebo, L., & Silverman, L. (1982). Model reduction via balanced state space representations. *IEEE Transactions on Automatic Control*, *27*(2), 382-387.
[45] Oppenheim, A., Mecklenbrauker, W., & Mersereau, R. (1976). Variable cutoff linear phase digital filters. *IEEE Transactions on circuits and systems*, *23*(4), 199-203.
[46] Mullis, C., & Roberts, R. (1976). Roundoff noise in digital filters: Frequency transformations and invariants. *IEEE Transactions on Acoustics, Speech, and Signal Processing*, *24*(6), 538-550.
[47] Koshita, S., Tanaka, S., Abe, M., & Kawamata, M. (2008). Gramian-preserving frequency transformation for linear discrete-time state-space systems. *IEICE Transactions on Fundamentals of Electronics, Communications and Computer Sciences*, *91*(10), 3014-3021.
[48] Koshita, S., Tanaka, S., Abe, M., & Kawamata, M. (2008, May). Gramian-preserving frequency transformation for linear discrete-time systems using normalized lattice structure. In *2008 IEEE International Symposium on Circuits and Systems (ISCAS)* (pp. 1124-1127). IEEE.
[49] Koshita, S., Abe, M., & Kawamata, M. (2018). Recent advances in variable digital filters. *Digital Systems*.
[50] Koshita, S., Abe, M., & Kawamata, M. (2010, October). Realization of variable low-pass state-space digital filters using step responses. In *2010 10th International Symposium on Communications and Information Technologies* (pp. 566-570). IEEE.
[51] Koshita, S., Kumamoto, Y., Abe, M., & Kawamata, M. (2013). Adaptive IIR band-pass/band-stop filtering using high-order transfer function and frequency transformation. *Interdisciplinary Information Sciences*, *19*(2), 163-172.